Conduction-band structure of alkali-metal-doped C_{60}

S. Satpathy,* V. P. Antropov,† O. K. Andersen, O. Jepsen, O. Gunnarsson, and A. I. Liechtenstein‡

Max-Planck-Institut für Festkörperforschung, Heisenbergstrasse 1, D-7000 Stuttgart 80, Federal Republic of Germany

(Received 3 December 1991; revised manuscript received 6 March 1992)

We discuss the geometries of crystalline fcc C_{60} for three cases of directional order, the hypothetical unidirectional structure with space group $Fm\bar{3}$, the bidirectional structure ($P4_2/mnm$) which is the ordered version of the structure observed for alkali-metal-doped compounds at room temperature, and the quadridirectional, low-temperature structure ($Pa\bar{3}$) of pure C_{60}. Analytical, parameter-free expressions for the t_{1u} wave functions are derived and used to obtain analytical conduction-band Hamiltonians for all three structures. The interactions with other subbands are included in numerical tight-binding calculations with a basis of 60 radial carbon orbitals per molecule. *Ab initio* density-functional [local-density approximation (LDA)] calculations are performed for unidirectional fcc C_{60} and RbC_{60} for different lattice constants. We use the linear-muffin-tin-orbitals (LMTO) method in the atomic-spheres approximation with carefully chosen interstitial spheres. The LDA bands are compared with photoemission and inverse photoemission data for C_{60}. For RbC_{60} we find that the alkali-metal atom is fully ionized and that the doped electron occupies the t_{1u} band in a rigid-band-like fashion. Tight-binding theory explains why, and indicates that this holds generally for $A_{n-x}B_xC_{60}$ with $n \leq 3$. The LDA calculation shows that, for a given structure, the conduction band scales uniformly in energy when, because of doping, the lattice constant a is changed. The energy scale behaves like $W \propto d(a)\exp[-d(a)/0.58\ \text{Å}]$ where d is the shortest distance between atoms belonging to different molecules. Both the LDA-LMTO and the tight-binding conduction bands are well fitted by the t_{1u} Hamiltonians. For a=14.1 Å the density of states for a conduction-band occupation of three electrons is 15, 17, and 21 electrons/(mol eV) for the unidirectional, bidirectional, and quadridirectional structures, respectively. The calculated Stoner exchange parameter is less than half the inverse density of states per spin and atom, but the Coulomb self-energy for a molecular orbital is presumably larger than the t_{1u} bandwidths, which are 0.52 eV (uni), 0.64 eV (bi), and 0.44 eV (quadri) for $a = 14.1$ Å. The LDA value (0.58 Å) for the decay of the intermolecular hopping was used together with experimental data for T_c vs a for $K_{3-x}Rb_xC_{60}$ compounds in the McMillan formula. The assumptions that the Coulomb interaction μ^*, the electron-phonon interaction $V_{e\text{-ph}}$, and the average phonon frequency ω are *all* independent of a were found to be inconsistent.

I. INTRODUCTION

The discovery of the C_{60} molecule,[1] of its condensation into an insulating solid,[2] and of superconductivity in the alkali-metal-doped solids $A_{n-x}B_xC_{60}$ (A and B are alkali-metal atoms and $n \leq 3$) (Ref. 3) have generated enormous interest in these systems. At room temperature, solid C_{60} forms a face-centered-cubic (fcc) structure in which the individual molecules rotate. Below 249 K orientational order develops[4] and at low temperature the structure is simple cubic (sc) with four different orientations.[5,6] In the doped systems the alkali-metal atoms enter the octahedral and tetrahedral sites. At room temperature, there seems to be two orientations, equally populated and randomly distributed on the fcc lattice.[7] Whether orientational order sets in at low temperatures is presently unknown. Upon doping, the distance between the molecules increases, and so does T_c (Ref. 8); it reaches a maximum which is presently 33 K and occurs for $RbCs_2C_{60}$.[9,10] For doping levels beyond 3, the structure becomes body-centered tetragonal or body-centered cubic, superconductivity disappears, and compounds with n=6 are insulators.[11]

This behavior is consistent with a one-electron picture in which the lowest unoccupied molecular orbital (LUMO) is threefold degenerate (t_{1u}) (Refs. 12 and 13) and in the solid broadens into a band which is isolated from the next higher band.[14] Furthermore, in order that the doped electrons enter the t_{1u} band, this picture assumes that the alkali-metal atoms neither deform the band appreciably nor induce an extra band below it. The behavior of T_c with doping should then mainly reflect the change of the electronic density of states at the Fermi level with occupancy and separation between molecules.

In this paper we shall present accurate *ab initio* local density-functional [local-density approximation (LDA)] calculations as well as analytical and numerical tight-binding (TB) calculations which support and add details to this picture. We first discuss the structures of molecular and solid forms of C_{60} in detail. For the molecule, we then derive analytical, parameter-free expressions for the t_{1u} molecular orbitals (MO's). For solids, where the C_{60} molecules are on a fcc lattice, we study the influence of orientational order on the conduction-band structure

using the tight-binding approximation at two levels of accuracy. At the lowest, where we take Bloch sums of the t_{1u} MO's as basis and only include hopping between nearest-neighbor *molecules*, we can derive analytical expressions for the band Hamiltonians. These could turn out to be useful for future studies of the Coulomb correlations and the electron-phonon interaction. The crystal structures studied are the unidirectional structure (space group $Fm\bar{3}$) considered in previous electronic-structure calculations, a bidirectional structure ($P4_2/mnm$) which may be realistic for the doped compounds, and the proper quadridirectional structure ($Pa\bar{3}$) of pure C_{60}.

We study the energy scale of the conduction band and its dependence on the lattice constant, as well as the influence of alkali-metal doping, by performing accurate *ab initio* calculations for C_{60} and AC_{60}, with A= K, Rb, or Cs, in the unidirectional structure. We use the LDA and the linear-muffin-tin-orbitals (LMTO) method in the atomic-spheres approximation (ASA) with carefully chosen interstitial spheres. The LDA bands for C_{60} are compared with recent photoemission and inverse photoemission data. Then we study the effects of doping. We find that the alkali-metal atom is fully ionized and that the doped electrons occupy the t_{1u} band in a rigid-band-like fashion. Our tight-binding t_{1u} model explains why, and indicates that this holds generally for $A_{n-x}B_xC_{60}$ with $n \leq 3$.

The LDA calculation of the conduction-band density of states is performed for three different lattice constants and we find that it scales uniformly. The energy scale as a function of the intermolecular separation calculated for the unidirectional structure can therefore be used to calibrate the TB results for the bidirectional and quadridirectional structures. We also calculate the value of the Stoner exchange parameter in the LDA and estimate that the bandwidth may be considerably reduced before a spin-density-wave instability sets in. Finally, we try to correlate the lattice-constant dependence of the density of states at the Fermi level with experimental data for T_c versus lattice constant for $K_{3-x}Rb_xC_{60}$ compounds using the McMillan formula. It turns out that the single-particle hopping considered by us cannot be the only important *intermolecular* interaction.

II. STRUCTURE AND BONDING

The C_{60} molecule forms a truncated icosahedron with 20 hexagonal and 12 pentagonal faces (Fig. 1 and Table I). Each atom is threefold coordinated and three of the four valence electrons occupy two-center σ-like bonding orbitals which are separated from their unoccupied antibonding counterparts by an energy gap of more than 15 eV starting 4 eV below the Fermi level.[12,13] The levels of interest are those around the Fermi level and their MO's are π-like and formed from 60 atomic orbitals (AO's) pointing in the radial direction. Due to the curvature of the C_{60} molecules, the σ- and π-like bonds are not formed exactly from, respectively, the sp^2 hybrids in the tangential plane and the p_z orbitals in the radial direction. Neither are they formed exactly from sp^3 hybrids, with one in the radial direction and three approximately in the nearest-neighbor directions.

Each atom is the common corner of two hexagons and one pentagon so that, of the three edges directed towards the neighbors, one is common to two hexagons (hexagon edge) and two are common to a pentagon and a hexagon

TABLE I. Atomic positions in C_{60} with y orientation, and the t_{1u} LUMO. We only include the nine sites $\mathbf{R} \equiv (X,Y,Z) \equiv (\hat{X},\hat{Y},\hat{Z})D/2$ which lie in the positive octant, because our t_{1u} partner functions have specific parities with respect to the XY, YZ, and ZX mirror planes (Fig. 1). The bond length is b, and the length difference between pentagon and hexagon bonds is neglected. The values given below in the three first columns are the positions in units of $b/2$. The ratio between the diameter and the bond length is $D/b = \sqrt{9\tau+10}$. The constant τ is the golden ratio $[\sqrt{5}+1]/2 \simeq 1.618$. The coefficients $c(1,Z)$ of the low-energy MO Eq. (18) are with high precision $\hat{Z}/10$. The coefficients of the hexagon-edge antibond approximation to the LUMO are $\tilde{c}(2,Z)$ listed in the fourth column. Orthogonalization of this function to the $\hat{Z}/10$ MO yields the high-precision LUMO with coefficients $c(2,Z)$ listed in the last column. The absolute values of the eight nonzero LUMO coefficient are named p to w in order of decreasing magnitude and their decimal values are given in Eq. (19).

$\hat{X}\times D/b$	$\hat{Y}\times D/b$	$\hat{Z}\times D/b$	$\tilde{c}(2,Z)\times\sqrt{80}$	$c(2,Z)\times\sqrt{80}D/b$	
0	1	3τ	0	-2	$-v$
3τ	0	1	2	6τ	p
1	3τ	0	0	0	o
1	$2+\tau$	2τ	τ	$3\tau+2$	r
2τ	1	$2+\tau$	$-(\tau-1)$	$-(3+\tau)$	$-t$
$2+\tau$	2τ	1	-1	$-(4\tau-1)$	$-s$
2	$2\tau+1$	τ	$-\tau$	$-(3\tau+4)$	$-q$
τ	2	$2\tau+1$	$(\tau-1)$	$3-\tau$	w
$2\tau+1$	τ	2	1	$2\tau+1$	u

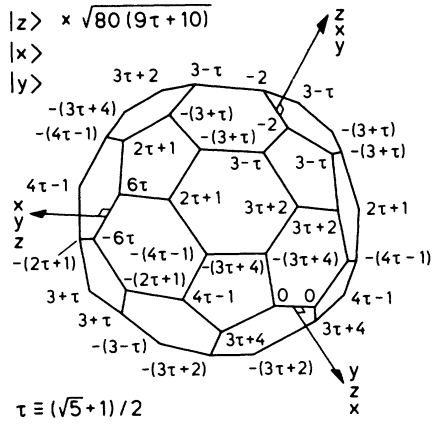

FIG. 1. C_{60} molecule and t_{1u} LUMO. The atomic coordinates are given in Table I. The choices of Cartesian coordinates and of t_{1u} partner functions are appropriate for a molecule with y orientation in the fcc unidirectional or bidirectional structures. These axes in configuration and t_{1u} space are used as local axes for all molecular orientations considered in the present paper. The numbers at the atoms are the c coefficients multiplying the radial AO's in the expansion (18) of the LUMO. They are listed in Table I. The coefficients on the far side of the molecule may be obtained from those in the front, by inversion and sign change. The three partner functions, labeled $|Z\rangle$, $|X\rangle$, and $|Y\rangle$, are orthonormal and related through rotations around [111]. Hence, the upper labels on the cubic axes are appropriate for $|Z\rangle$, the middle labels for $|X\rangle$, and the lower labels for $|Y\rangle$. The symmetry of the functions is such that a function labeled $|Z\rangle$ is even under reflection in the xz and yz mirror planes, and odd under reflection in the xy mirror plane.

(pentagon edges). The 30 occupied π-like MO's are approximately hexagon-edge bonding and the 30 unoccupied ones antibonding. The crudest picture of the bonding in the C_{60} molecule is therefore one with single bonds along pentagon edges and double bonds along hexagon edges. The experimental bond lengths, b_p and b_h, differ by only 0.06 Å and they agree reasonably well with those obtained from the Pauling formula using bond orders calculated in the LDA with the LMTO method.[12]

The presence of two different bond lengths does not break the icosahedral symmetry. The length of the icosahedron edge is

$$2b_p + b_h \equiv 3b \tag{1}$$

and the pentagons appear by capping the icosahedron corners at the distance b_p measured along the edge. The remaining middle piece of the edge, with length b_h, is the hexagon edge. Its distance to the center of the molecule (the radius of the sphere touching the hexagon edge) therefore only depends on the average bond length b, defined as in (1). In fact, the diameter of this sphere touching the hexagon edges is $D_{\min} = 3\tau b \approx 4.85b$, where

$$\tau \equiv (\sqrt{5}+1)/2 = 2\cos(\pi/5) \approx 1.618 \tag{2}$$

is the ratio of the golden section ($1/\tau = \tau - 1$). The diameter of the sphere passing through the atoms, i.e., the diameter of the C_{60} molecule, does depend on $b_p - b_h$, but only weakly: If the bond-length difference were vanishing, the C_{60}-molecule diameter would be

$$D \equiv 2R = b\sqrt{9\tau+10} = b\sqrt{(3\tau)^2+1} \approx 4.96b. \tag{3}$$

Now that b_h is (slightly) smaller than b_p, the pentagons are pushed inwards so that the atoms are on a sphere whose diameter is (slightly) smaller than D, but (considerably) larger than $D_{\min}$. Therefore, we shall keep referring to D as defined through Eqs. (3) and (1) as the diameter of the molecule.

According to a recent measurement,[6] the bond lengths in solid C_{60} at low temperatures are

$$b_p = 1.455 \text{ and } b_h = 1.391 \text{ Å}. \tag{4}$$

These values were used in the numerical tight-binding and LDA calculations of the present paper (except in Figs. 11–13). The analytical expressions employed the same value for both bond lengths. Provided that this value is obtained from (1), i.e.,

$$b = 1.434 \text{ Å and } D = 7.105 \text{ Å}, \tag{5}$$

this approximation is surprisingly accurate.

In *solid* fcc C_{60} the smallest distance d between atoms belonging to different molecules satisfies

$$d \geq (a/\sqrt{2}) - D, \tag{6}$$

with a being the cubic lattice constant. Upon doping, the latter increases from 14.04 to 14.49 Å when going from C_{60} to Rb_2CsC_{60}, while the size of the molecule remains comparatively constant. The intermolecular distance d is therefore twice the intramolecular bond length b, or more. As a consequence, the hopping interaction between the molecules is weak and essentially only via the radial AO's. This interaction is, however, extremely sensitive to the geometry of the contact region and it has been argued on the basis of TB calculations that this interaction provides an important contribution to the orientational energy.[15] We shall therefore have to discuss the contact geometries for the three cases of orientational order considered in this paper.

A. Unidirectional and bidirectional structures

Figure 2 (and also Fig. 1) shows the molecule oriented in the fcc unidirectional structure, i.e., with 8 of its 20 threefold axes (denoted by solid triangles) coinciding with the cubic [111] axes and with 3 of its 15 twofold axes coinciding with the cubic [100] axes. Since in cubic symmetry the [100] axes are fourfold, there are two possible orientations of the molecule: the "top hexagon-edge" (the one with the highest z value) can either be parallel with the x or with the y axis. In Fig. 2, as well as in Fig. 1 and in Table I, the y orientation has been chosen.

In Fig. 2 the dots mark those atoms which are in closest contact (at distance d) with atoms in a neighboring molecule. These closest contact atoms belong to those pentagon edges whose centers lie approximately in the [011] directions. Since the direction from the molecule center to the pentagon-edge center near, e.g., [011] is slightly closer to the y axis than to the z axis, the hopping integral between the radial AO's on the contact atoms is slightly larger when the two molecules are oriented perpendicular to each other than when they have the same orientation. For electron-doped C_{60} this effect was found in the TB calculation Ref. 15 to destabilize the unidirectional fcc crystal (space group $Fm\bar{3}$) with respect to a crystal in which the molecules remain on the fcc sites but their orientation alternates from one (001) plane to the next. In this bidirectional crystal (space group $P4_2/mnm$), the hopping integral is increased for the largest possible number of nearest neighbors, i.e., for 8 of the 12. Such a structure with equal population of the two directions was also deduced from room-temperature x-ray-diffraction data for the *doped* compounds K_3C_{60},[7] although in that case the orientations were found to be disordered. So far the ordered bidirectional structure has not been observed, but since the x-ray scattering does not resolve short-range order below about 20 Å, we believe that not only the hopping integrals that we shall deduce for this structure, but even the density of states are relevant.

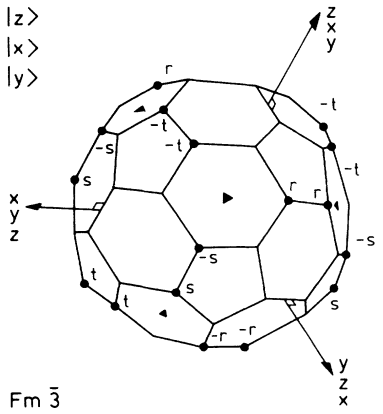

FIG. 2. y-oriented C_{60} molecule in the unidirectional or bidirectional structure ($Fm\bar{3}$ or $P4_2/mnm$) as in Fig. 1 and Table I. For an x-oriented molecule, the global translation axes are rotated by $+90°$ around the z axis. The dots mark those atoms which are closest to an atom in a neighboring molecule (contact atoms) and only the corresponding LUMO coefficients r, s, and t have been given. The cubic axes are twofold axes and triangles denote the threefold axes. The octahedral and tetrahedral sites for alkali-metal dopants are, respectively, $a/2$ away from the center of the molecule along a cubic axis and $a\sqrt{3}/4$ away along a threefold axis.

In the following, we shall be using a *global* as well as *local* coordinate systems. The global system has its axes along the cubic translation axes. A local system is centered at a particular molecule and is oriented as in Figs. 1 and 2. Hence, for a y-oriented molecule, the local and global axes coincide, but for an x-oriented molecule, which is rotated by $-90°$ around the z axis, the global axes are rotated with respect to the local axes by $+90°$ around the z axis. Coordinates in the global and local systems will be denoted (x, y, z) and (X, Y, Z), respectively.

In order to find the dependence of the hopping integrals on the lattice constant and on the orientational order, we need to specify the contact geometries. As seen from Fig. 2 and Table I, the position of a contact atom on the y-oriented molecule at the origin is $\mathbf{R}_1 = (1, 2+\tau, 2\tau)b/2$ and the position of its nearest neighbor on the x-oriented molecule is $\mathbf{R}_2 = (1, -2\tau, -2-\tau)b/2$ in the global system, but relative to the center $(0,1,1)a/2$ of this molecule. The vector distance between these closest contact atoms on molecules with perpendicular orientation is therefore

$$\begin{aligned}\mathbf{d}_\perp &\equiv (a/2)[0,1,1] + \mathbf{R}_2 - \mathbf{R}_1 \\ &= [(a/2) - (1+3\tau/2)b]\,[0,1,1] \\ &\approx [(a/\sqrt{2}) - 0.978D]\,[0,1,1]/\sqrt{2}. \end{aligned} \tag{7}$$

Had the second molecule been y oriented, the position of its closest contact atom would have been $\mathbf{R}_2 = -(-1, 2+\tau, 2\tau)b/2$ and the vector distance accordingly

$$\begin{aligned}\mathbf{d}_\parallel &\equiv (a/2)[0,1,1] - b[0, 2+\tau, 2\tau] \\ &= \mathbf{d}_\perp + (1-\tau/2)b[0,-1,1] \\ &\approx \mathbf{d}_\perp + 0.055D[0,-1,1]/\sqrt{2}. \end{aligned} \tag{8}$$

Comparing with (6) we note that for these edge-to-edge contacts the "effective" molecule diameter is a few percent smaller than D, e.g., the contact distance is $d_\perp \approx (a/\sqrt{2}) - 0.978D$ for perpendicular molecules. Secondly, for such molecules the vector distance is in the fcc nearest-neighbor direction. Finally, for parallel molecules, the increment $\mathbf{d}_\parallel - \mathbf{d}_\perp$ is perpendicular to $\mathbf{d}_\perp$ so that the closest separation is now a bit larger: $d_\parallel^2 \approx d_\perp^2 + (0.055D)^2$. Using the data D=7.105 Å and a=14.04 Å appropriate for pure C_{60}, we find that $d_\perp$=2.980 Å and that $d_\parallel$ is 0.8% larger.

B. Quadridirectional structure

The low-temperature structure of pure C_{60} was solved recently:[6] the molecules are centered on a fcc lattice like in the unidirectional and bidirectional structures but the translation cell is sc with four orientations per cell and the space-group symmetry is $Pa\bar{3}$. With respect to the local axes of the molecule at the origin, the translation axes are rotated by an angle $\varphi \approx 22°$ around the +[111] axis, which is then the only conserved threefold axis through the origin of the sc cell. The new translation axes are shown in Fig. 3. In the notation of Ref. 6, $\varphi \equiv 120° - \phi$. The orientation of the molecules at $(1,1,0)a/2$, $(0,1,1)a/2$, and $(1,0,1)a/2$ may be obtained by rotating the molecule at the origin by 180° around, respectively, the x, the y, and the z axis. The conserved threefold axis is thus $[1\bar{1}\bar{1}]$ for the molecule at $(1,1,0)a/2$, $[\bar{1}1\bar{1}]$ for the molecule at $(0,1,1)a/2$, and $[\bar{1}\bar{1}1]$ for the molecule at $(1,0,1)a/2$.

As indicated in Fig. 3, this quadridirectional structure succeeds in making all intermolecular contacts equivalent but not symmetric. A contact is between one of the 6 pentagons neighboring the conserved threefold axis and one of the hexagon edges belonging to the equatorial zig-zag line which runs perpendicular to this threefold axis and which consists of 6 hexagon and 12 pentagon edges. The angle of rotation φ is determined by the condition that all contacts be equivalent. This means that all contact pentagons (and all the contact-hexagon edges) should be equivalently positioned with respect to the nearest-neighbor direction, i.e., to the appropriate [011] direction. The $x = y$, the $y = z$, and the $z = x$ planes must therefore coincide with the appropriate mirror planes of the molecule. This leads to the value

$$\varphi = \arctan(\sqrt{3}/\tau^3) \approx 22.24° \tag{9}$$

and, hence, $\cos\varphi = \tau^2/\sqrt{8}$. This value deviates slightly from the 22.38° defined as the ideal in Ref. 6. The reason is that at this level of accuracy, which is well beyond the experimental uncertainty of about one degree in φ, the definition of "ideal" is arbitrary because the icosahedral symmetry of the molecule is weakly broken in the solid. As a consequence, the $x = y$, $y = z$, and $z = x$ mirror planes are not exact.

The contacts in the unidirectional and bidirectional structures have a mirror plane perpendicular to the contact, e.g., the yz plane for the [011] contacts. In the quadridirectional structure this is not the case and the two pairs of contact atoms have different separations, d_ϕ and $d_{\phi 2}$. We now seek the vector separation for the closest pair: For the pentagon pointing towards [011], the corresponding contact atom is the same as the one considered in the unidirectional and bidirectional structures. Its position is $\mathbf{R}_1 = (1, 2+\tau, 2\tau)b/2$ in the local coordinate system and, hence, with the use of (9), $\mathbf{R}_1 = (1+\tau-\sqrt{2},\ 1+\tau+\sqrt{2},\ 1+\tau)\,b/2$ in the global system. In Fig. 3(a) this atom has a label r. The closest hexagon-edge contact atom on the molecule at $(0,1,1)a/2$ is the one which, translated and rotated around the y axis, back to the molecule at the origin, appears in Fig. 3(a) on the upper-left-hand side of the (111) equator, carries a label r, too, and has the position $(1, -2-\tau, 2\tau)b/2$ in the local system. In the global system, and rotated back to the orientation appropriate for site $(0,1,1)a/2$, the position is $\mathbf{R}_2 = [1-(1-\sqrt{2})\tau,\ -1+(1-4\sqrt{2})\tau,\ 1-(1+5\sqrt{2})\tau]\,b/6$. For the vector distance we therefore obtain

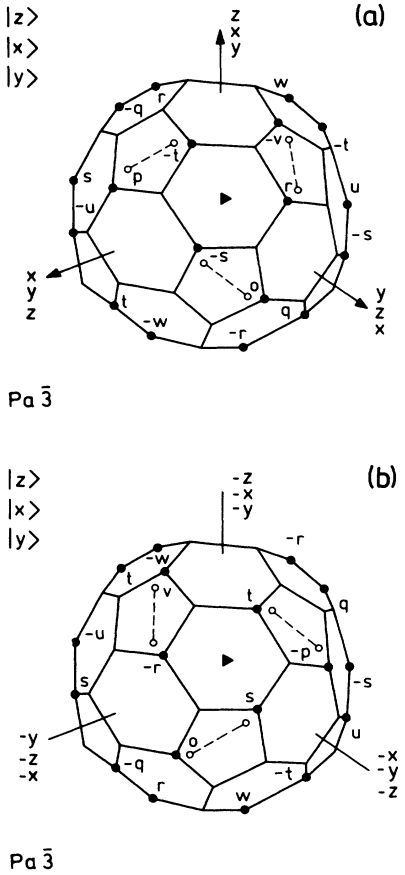

FIG. 3. (a) C_{60} molecule at the origin of the sc translation cell for the quadridirectional structure ($Pa\bar{3}$). Compared with the previous figures, the translation axes have been rotated around the +[111] axis by $\varphi \approx 22°$. Out of the four threefold axes through the origin, only the [111] axis has been conserved and is labeled by a triangle. The molecules at $(1,1,0)a/2$, $(0,1,1)a/2$, and $(1,0,1)a/2$ are rotated with respect to the one at the origin by 180° around the x, y, and z axes, respectively. The dots mark those atoms which are nearest and next nearest to an atom in a neighboring molecule, and only these LUMO coefficients have been given. For each molecule, we have chosen the LUMO partner functions to equal those shown in Fig. 1, i.e., we use functions glued to the molecule. All contacts are equivalent and consist of a pentagon neighboring the conserved threefold axis and a hexagon edge at the "(111) equator." The contact hexagon edges of the neighboring molecules are indicated by dashes. The octahedral and tetrahedral sites are, respectively, $a/2$ away from the center of the molecule along a cubic translation axis and $a\sqrt{3}/4$ away along a [111] axis. (b) Same as (a), except that the molecule is viewed from behind.

$$\mathbf{d}_\phi \equiv (a/2)[0,1,1] + \mathbf{R}_2 - \mathbf{R}_1$$
$$= (a/2)[0,1,1] - (b/6)\,[(2-3\sqrt{2}) + \tau(4-\sqrt{2}), (4+3\sqrt{2}) + \tau(2+4\sqrt{2}),\ 2+\tau(4+5\sqrt{2})]$$
$$\approx [(a/\sqrt{2}) - 0.964D]\,[0,1,1]/\sqrt{2} + 0.067D\,[-0.97, -0.18, 0.18]\,. \qquad (10)$$

As in Eq.(8), the projections are onto the fcc nearest-neighbor direction and a plane perpendicular to it. The squared distance is therefore $d_\phi^2 \approx [(a/\sqrt{2}) - 0.964D]^2 + (0.067D)^2$. For this face-to-edge contact, the shortest distance is larger, or the effective molecule diameter shorter, than for the edge-to-edge contacts found in the unidirectional and bidirectional structures. In fact, with a=14.04 and D=7.105 Å, we obtain d_ϕ=3.115 Å, which is 4.5% larger than $d_\perp$. The experimental distance[6] derived without assuming that the molecules have icosahedral symmetry and equal bond lengths is d_ϕ= 3.12 Å, i.e., almost identical with our value.

The second-closest separation $d_{\phi 2}$ is between the contact atoms labeled $-v$ and $-q$ in Fig. 3(a) and is experimentally[6] 4.8% larger than the closest separation d_ϕ and, hence, 9% larger than $d_\perp$. The remaining intermolecular atom separations are distinctly larger. With our simplifying and quite accurate assumptions that the molecules have icosahedral symmetry and equal bond lengths, we shall now discuss the geometry of this asymmetric contact a bit further.

We first wish to show that the mirror plane of the molecule at the origin, which reflects the (r to $-v$) pentagon diameter onto itself, is parallel (but not coinciding) with the mirror plane of the molecule at (0,1,1)a/2, which reflects the contacting hexagon edge (dashed line between open dots) onto itself. To prove this, we first note that the operations required to take the former mirror plane into the latter are a +120° rotation around the threefold axis, followed by a 180° rotation around the y axis and, finally, a translation by (0,1,1)a/2. (The two latter are not symmetry operations of the molecule.) Using Table I, it is then easy to show that the mirror planes of the two sides of the contact would be parallel if the turn angle were $\varphi = \arccos[(3\sqrt{\tau+2} - 2)/4] = 22.09°$. To the experimental accuracy, this is true. One consequence is that the pentagon diameter is parallel with the hexagon edge. In fact, the experimental paper[6] noted that the angle between the two is 0.4°. This means that the four contact atoms form an elongated trapezium where the short parallel edges are of lengths τb (pentagon diameter) and b (hexagon edge), and where the remaining long edges are of lengths d_ϕ and $d_{\phi 2}$.

We can now find the second-nearest separation $d_{\phi 2}$. The distance between the two parallel mirror planes is $a(2-\tau)/[4\tau\sqrt{2+\tau}]$. If the a/b ratio were $2\sqrt{2+\tau}/(2-\tau) \approx 9.96$, this distance would equal $(\tau-1)b/2$ and, consequently the d_ϕ edge would be perpendicular to the parallel edges of the trapezium. The second-closest separation would therefore be given by

$$d_{\phi 2}^2 = d_\phi^2 + [(\tau-1)b]^2. \qquad (11)$$

This holds exactly for a=9.96b=14.28 Å and, approximately, for the real lattice constant of pure C_{60}. For the second-nearest separation, (11) yields $d_{\phi 2}$=3.24 Å as compared with the experimental value[6] of 3.27 Å. This slight discrepancy is mainly caused by the fact that the experimental molecule has a whole spectrum of intramolecular bond lengths, and not merely one (or two).

In the TB calculation Ref. 15 this quadridirectional structure was found to give a favorable kinetic energy. First, the (hypothetic) case was considered where the hopping integrals corresponding to the distances d_ϕ and $d_{\phi 2}$ were equal, and equal to the nearest-neighbor hopping integral in the unidirectional structure, while hopping between more distant neighbors was neglected. In this case, the hopping energy was found to be about 20% lower in the quadridirectional than in the unidirectional structure due to favorable phase factors of the MO's for this face-to-edge contact, leading to good-sized overlaps between occupied MO's on one molecule and unoccupied MO's on the other. For edge-to-edge and face-to-face contacts such overlaps are often small, because occupied MO's tend to be bonding and unoccupied MO's to be antibonding between nearest-neighbor atoms inside the molecule (that is what causes the intramolecular two-center bonds). However, by placing a hexagon edge *across* a pentagon face, such a cancellation of AO pair contributions does not occur: The higher *occupied* MO's have a phase of $\approx 2 \cdot 2\pi/5$ between pentagon *second*-nearest neighbors and this matches reasonably well with the phase $\approx \pi$ between the hexagon-edge atoms for the *unoccupied* MO's. Moreover, the phase angle $\approx 4 \cdot 2\pi/5$ between second-nearest pentagon neighbors for the higher unoccupied MO's matches the phase angle ≈ 0 of the hexagon-edge bonding MO's reasonably well.

When taking into account that for geometrical reasons $d_\phi < d_{\phi 2}$, the relative energy of the quadridirectional and unidirectional structures depends also on the repulsive forces which determine the intermolecular separations. For the extreme case of a hard-core repulsion which fixes $d_\phi = d_\parallel$ (by adjustment of the lattice constant for constant φ), the quadridirectional structure was found to be unfavorable due to the reduced hopping across the second pair of contact atoms. For the intermediate case where the repulsion fixes the average distances to be the same, $(d_\phi + d_{\phi 2})/2 = d_\parallel$ or $d_\perp$, the quadridirectional structure was found to have the lowest energy of all three structures.[15] The quadridirectional structure, furthermore, benefits from the isotropic part of the van der Waals interaction. The reason is that for, e.g., a hard-core repulsive potential, the separations of the centers of the molecules are smaller in the quadridirectional structure, and the van der Waals interaction is therefore more attractive. (Note, that in the orientational-energy problem the lattice constant is a variable which should

be minimized together with the orientation. This differs from the point of view of the present paper where we seek the conduction-band structure at the experimentally well-known lattice constants and for different orientational orders.)

III. TIGHT-BINDING CALCULATIONS

In this section we present tight-binding (TB) calculations of the conduction-band structure of pure C_{60} in the unidirectional, bidirectional, and quadridirectional structures, anticipating LDA results to be presented in Secs. IV B and IV C concerning the rigidity of the conduction band under alkali-metal doping and its dependence on the lattice constant.

We have performed electronic-structure calculations at essentially three levels of accuracy. At the highest, the *ab initio* LDA-LMTO level, we are presently only able to perform the calculations for one molecule per cell, that is, for the unidirectional structure. Since the LDA-LMTO calculations are charge-self-consistent they are well suited for studying the influences of the alkali-metal dopants and of the changes of lattice constant. At the second level, we can perform numerical calculations also for the bidirectional and quadridirectional structures, but only for pure C_{60}, because we use the empirical TB method with a basis consisting of merely the 60 radial AO's per molecule. The hopping integrals are those used in the study[15] of orientational ordering, and they were obtained by fitting to the overall π-band structure of an LDA-LMTO calculation for unidirectional C_{60}. The limitation to undoped C_{60} is due to our ignorance about the hopping matrix elements to the alkali-metal atoms and is justified by the results of the LDA-LMTO calculations for doped crystals. At the third level, we are able to perform the TB calculations *analytically* because we use a basis set of just the three t_{1u} MO's per molecule. These analytical, single-MO calculations provide insights and they result in band Hamiltonians which can fit the available LMTO and TB calculations with good accuracy. They can therefore be used for extrapolation to the more complicated structures. The present section deals with the TB calculations of the second and third levels, which we shall refer to as, respectively, the radial-AO and the single-MO approximations.

The TB calculations employ a basis set with one radial orbital per carbon atom. The on-site elements of the one-electron Hamiltonian are all identical. For the hopping integral between the radial orbitals on atoms 1 and 2 we use the following form, valid for *pp* hopping:

$$V_{12} = [V_\sigma(d) - V_\pi(d)](\hat{\mathbf{R}}_1 \cdot \hat{\mathbf{d}})(\hat{\mathbf{R}}_2 \cdot \hat{\mathbf{d}}) + V_\pi(d)(\hat{\mathbf{R}}_1 \cdot \hat{\mathbf{R}}_2). \tag{12}$$

Here, $\hat{\mathbf{R}} \equiv \mathbf{R}/R$ is a unit vector in the radial direction and $\hat{\mathbf{d}} \equiv \mathbf{d}/d$ is a unit vector in the direction from atom 1 to atom 2. For the ratio between the σ and π integrals we take the value -4 recommended by Harrison.[16] The distance dependence we parametrize as

$$V_\sigma(d) = -4V_\pi(d) = (d/d_0)V_0 \exp[-(d-d_0)/L]. \tag{13}$$

As in Ref. 15, we use the parameter values

$$L = 0.505 \text{ Å}, \; V_0 = 0.90 \text{ eV}, \text{ and } d_0 \equiv 3.00 \text{ Å}, \tag{14}$$

and we truncate the hopping after the nearest neighbors *inside* but not between the molecules; the appropriate π-like intramolecular hopping integrals are thus $V_h = -2.78$ eV and $V_p = -2.59$ eV. The parameters were determined by fitting the width of the entire π-like band and the widths of the subbands near the gap in unidirectional C_{60} to the results of a LDA-LMTO calculation.[15] The value of L was thus determined by the ratio of the π-band width to the average subband widths. As we shall see in Sec. III B, this value gives a conduction-band dispersion in good agreement with the one given by the LDA-LMTO calculations for the unidirectional structure. In order to reproduce the dependence on the lattice constant, a more appropriate value would be L=0.58 Å (see Sec. IV C), provided that the intramolecular hopping integrals are unchanged.

We perform the numerical calculations with the molecule geometry given by (4) and with the *same* lattice constant, chosen to be a=14.10 Å, for all three cases of orientational order. The extrapolation to other lattice constants will be considered in Sec. IV C. For 14.10 Å, the values of the intermolecular hopping integrals for the near-neighbor contact atoms can be found from Eqs. (12), (13), and (14), using the contact geometries derived in the previous section, to be

$$V_\perp = 816, \; V_\parallel = 742, \; V_\phi = 597, \text{ and } V_{\phi 2} = 508 \text{ meV}. \tag{15}$$

In the order mentioned, the hopping integrals decrease by 10%, 22%, and 20%. This is due partly to the increase of the corresponding distances through Eq. (13) and partly to the variation in the alignment of the radial orbitals through Eq. (12). The near distances, as given by the expressions in the previous section, are

$$d_\perp = 3.02, \; d_\parallel = 3.05, \; d_\phi = 3.16, \text{ and } d_{\phi 2} = 3.28 \text{ Å}, \tag{16}$$

and, as was the case for a = 14.04 Å, they increase in the order mentioned by 0.8%, 4%, and 4%. Since according to (13) the decay of the hopping integral with distance has the logarithmic derivative

$$P = 1 - d/L \approx -5, \tag{17}$$

the distance-induced decrease is 4%, 20%, and 20%. Therefore, the 10% increase of the AO hopping integral achieved for 8 of the 12 nearest-molecule neighbors when going from the unidirectional to the bidirectional structure is partly due to the decreased distance, and partly to the improved alignment of the AO's. When going from the parallel to the quadridirectional orientation, the 22% decrease of the largest hopping integral, and the additional 20% decrease of the second largest, are due to increased distances.

A. The t_{1u} LUMO

The relatively large distance between neighboring molecules ($d/b \geq 2$) causes a relatively weak hopping between them ($V_d/V_b \leq 0.3$) so that the states of the crystal are approximately Bloch sums of linear combinations of *degenerate* MO's only (single-MO approximation). That is, the mixing in the crystal between Bloch states derived from different irreducible representations of the icosahedral group can, for many purposes, be neglected. We now give analytical, parameter-free expressions for the LUMO's, which will enable us to derive analytical expressions for the dispersions of the unidirectional, bidirectional, and quadridirectional conduction bands.

Considering the Hilbert space with 60 radial AO's per molecule, there are two threefold degenerate t_{1u} MO's, $|1,M\rangle$ and $|2,M\rangle$, with M=1,3. The latter, high-energy MO is the LUMO. If we expand a t_{1u} MO in AO's, $|i\rangle$ with i from 1 to 60, viz.,

$$|I,M\rangle = \sum_i |i\rangle\, c_i(I,M), \tag{18}$$

and then expand the coefficients in real spherical harmonics with respect to the center of the molecule, $c_i(I,M) = \sum_{lm} Y_{lm}(\hat{\mathbf{R}}_i) C_{lm}(I,M)$, only the coefficients with l=1 and 5 are different from zero. (Components with $l > 5$ do not contribute when $\hat{\mathbf{R}}$ are on the 60 discrete points.) Consequently, the low-energy MO, $|1,M\rangle$, has almost exclusively l=1 character, $C_{lm}(1,M) \propto \delta_{l,1}\delta_{m,M}$. We now choose the t_{1u} partner functions such that $|1,M\rangle$ are the real spherical harmonics in our chosen local coordinates (Fig. 1). $c_i(1,M)$ are therefore proportional to X, Y, and Z as given in Table I.

A first approximation to the LUMO, $|2,M\rangle$, may now be generated by projection of an antibonding two-center hexagon-edge orbital onto t_{1u} symmetry. Its coefficients, denoted $\tilde{c}(2,M)$, are given in the fourth column of Table I. Subsequent orthogonalization of this function to $|1,M\rangle$ results in a highly accurate LUMO whose coefficients $c_i(2,Z)$ are given in the fifth column of Table I, as well as in Fig. 1. This is the LUMO that we shall use to form conduction-band wave functions from, in the single-MO approximation. Its c coefficients are numbers, independent of the hopping interactions and the size of the C_{60} molecules.

The orthonormal partner functions, $|I,X\rangle$ and $|I,Y\rangle$, are obtained as shown in Fig. 1 by rotation of $|I,Z\rangle$ around one of the threefold [111] axes. This choice of t_{1u} partner functions, which will turn out to simplify the band Hamiltonian for the unidirectional and bidirectional structures considerably, is such that $|I,Z\rangle$ is even with respect to the twofold Z axis but odd with respect to the twofold X and Y axes or, in other words, $|I,Z\rangle$ is even with respect to the ZX and ZY mirror planes but odd with respect to the XY mirror plane. We therefore only need to specify the c coefficients when $X \geq 0$, $Y \geq 0$, and $Z \geq 0$, and since there are only nine such sites and one of these is on a nodal plane, any set of degenerate t_{1u} functions is specified by just eight c coefficients. These we denote by the letters p to w, chosen in such a way that for the LUMO they are positive and in order of decreasing amplitude. Their definition is given in the last column of Table I and their decimal values are

$$\begin{aligned} p &\approx 0.219 \ [0.224], \\ q &\approx 0.200 \ [0.181], \\ r &\approx 0.155 \ [0.181], \\ s &\approx 0.123 \ [0.112], \\ t &\approx 0.104 \ [0.069], \\ u &\approx 0.096 \ [0.112], \\ v &\approx 0.045 \ [0.000], \\ w &\approx 0.031 \ [0.069]. \end{aligned} \tag{19}$$

Here, the numbers in parentheses refer to the hexagon-edge antibonding LUMO before orthogonalization to the lower MO. Since the conduction-band width will be proportional to the product of the c coefficients for the contact atoms, this latter approximation is too inaccurate.

The *exact* LUMO may be obtained by diagonalizing one of the 2 × 2 matrices $\langle I,M|H|J,M\rangle$. For a nearest-neighbor Hamiltonian (and equal bond lengths) this exact result only deviates a few percent from the one in (19), e.g., $r \approx 0.153$, $s \approx 0.124$, and $t \approx 0.107$. This reflects the high accuracy of approximating $|1\rangle$ by the $l = 1$ spherical harmonics. Expressing the LUMO by the values in Fig. 1 will therefore suffice.

In the remainder of this paper we shall only be concerned with the LUMO, not with the low energy t_{1u} MO, and we therefore drop the index I.

B. Unidirectional conduction band

In Fig. 4 we show the conduction bands of C_{60} in the unidirectional fcc structure calculated with the TB method in the radial-AO approximation. The corresponding *ab initio* LDA-LMTO bands for RbC_{60} are shown in Fig. 5 and a comparison of the two proves the relevance of the TB bands. It should be kept in mind that the TB parameters (14) were chosen to fit the overall π-band structure rather than the details around the gap. The zero of energy is in both cases taken at the top of the valence band. We shall now provide a detailed understanding of these bands by going to the single-MO approximation.

In the single-MO approximation the Bloch functions are formed from the three LUMO's. If we restrict the intermolecular hopping to between nearest-neighbor *molecules*, which is an exceedingly good approximation, the conduction-band Hamiltonian is given by

$$\begin{aligned} \langle Z|H|Z\rangle = 4[\, & V_{\parallel}(rr)\cos(k_y a/2)\cos(k_z a/2) \\ & -V_{\parallel}(ss)\cos(k_x a/2)\cos(k_y a/2) \\ & +V_{\parallel}(tt)\cos(k_z a/2)\cos(k_x a/2)]\ , \end{aligned} \tag{20}$$

$$\langle Y|H|Z\rangle = 4V_{\parallel}(rt)\sin(k_y a/2)\sin(k_z a/2).$$

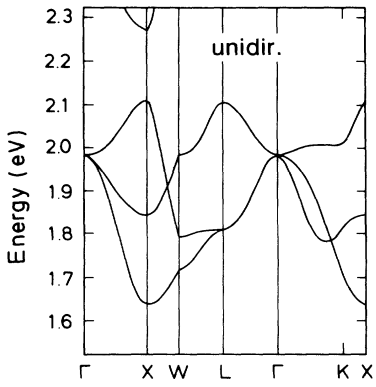

FIG. 4. C_{60} conduction band in the fcc unidirectional structure (space group $Fm\bar{3}$) with a=14.1 Å calculated in the radial-AO TB approximation. The coordinates of the high-symmetry points in the fcc Brillouin zone are Γ (0,0,0), X (2,0,0)π/a, W (2,1,0)π/a, L (1,1,1)π/a, K (3/2,3/2,0)π/a, and X (2,2,0)π/a. The zero of energy is at the top of the valence band and the parameters in (14) and (4) were used. The Fermi levels for dopings of one, two, three, and four electrons per molecule are, respectively, 1.76, 1.80, 1.85, and 1.95 eV. The density of states is shown in Fig. 7. Table II gives a fit to this band structure. Scaling to other lattice constants is explained in Sec. IV C.

Here, the zero of energy is taken at the LUMO energy, which is the center of gravity for the three bands. If we further restrict the range of the intermolecular hopping to between nearest-neighbor atoms, the conduction-band Hamiltonian depends on the coefficients of the contact orbitals only (see Fig. 2) and

$$V_{\parallel}(c_1c_2) = c_1V_{\parallel}c_2 + c_1V_{\parallel}c_2 \tag{21}$$

is the integral for hopping from a pentagon edge with LUMO amplitude c_1 on both atoms, to the neighboring pentagon edge with amplitude c_2 on both atoms, including only the two direct (not the diagonal) AO hoppings. The values of the integrals for hopping between LUMO's in this nearest-neighbor atom (NN) approximation (21) may be obtained from Eq. (15) and Table I, or Eq. (19), and are given in the first column of Table II.

The remaining matrix elements of the Hamiltonian (20) may be obtained by cyclic permutations of X, Y, and Z and, simultaneously, of k_x, k_y, and k_z. Its simple form is due to the facts that hopping beyond nearest-neighbor molecules can safely be neglected, and that the xy, yz, and zx mirror planes, with respect to which our t_{1u} partner functions have definite parities, are conserved in the crystal. As seen in Fig. 2, these mirror planes are perpendicular to the contacts and the $(ss+ss)$ contact is odd while the $(rr+rr)$ and $(tt+tt)$ contacts are even.

When we allow hopping beyond nearest-neighbor atoms, but not beyond nearest-neighbor molecules, Eq. (21) is replaced by

$$V_{\bowtie}(c_1c_2) = \sum_{ij} c_iV_{ij}c_j, \tag{22}$$

where i runs over the atoms near the contact of the first molecule and j runs over the atoms of the second, neighboring molecule. The subscript $\bowtie$ characterizes the geometry of the contact, and c_1c_2 characterizes the overlap of the LUMO's in the contact. (We shall use odd numbers for i and even for j.) When the sum in (22) extends beyond nearest neighbors, $V_{\bowtie}(rt)$ does, of course, not equal the geometrical average of $V_{\bowtie}(rr)$ and $V_{\bowtie}(tt)$ as in (21).

In the second column of Table II we give the converged values of the LUMO hopping integrals (22) using again the hopping parameters (14) chosen for the numerical TB calculations. By comparison with the results in the first column, the nearest-neighbor approximation is seen to be reasonably well converged. The worst case is the hopping across the $(tt+tt)$ contact (see Figs. 1 and 2) where, in addition to the positive contribution $\propto 2tt$ from diagonal hops across the pentagon-edge to pentagon-edge contact,

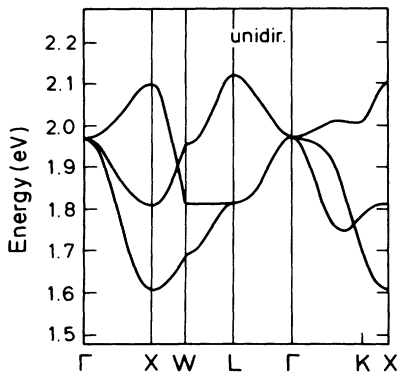

FIG. 5. RbC_{60} conduction band in the fcc unidirectional structure with a=14.1 Å calculated *ab initio* with the LDA-LMTO method. The zero of energy is at the top of the valence band. The density of states is shown in Fig. 8. The Fermi level is at 1.75 eV and the levels holding two and three electrons per molecule are at 1.81 and 1.86 eV, respectively. See the caption of Fig. 4.

TABLE II. t_{1u}-hopping integrals (single-MO approximation) and effective W and real W_X bandwidths derived herefrom for the unidirectional structure and a=14.10 Å. The t_{1u} hopping integrals listed in the columns radial-AO and LDA were fitted as described in the text to the conduction bands of C_{60} and RbC_{60} calculated with, respectively, the TB method in the radial-AO approximation and the LMTO method in the LDA. Scaling to other lattice constants is explained in Sec. IV C [Eqs. (47) and (48)].

	Single MO		Radial AO	LDA
(meV)	Nearest neighbor	Conv.	Fig. 4	Fig. 5
$4V_{\parallel}(rr)$	142	159	150	171
$4V_{\parallel}(ss)$	90	84	85	79
$4V_{\parallel}(tt)$	64	23	20	23
$4V_{\parallel}(rt)$	96	101	100	105
W	390	400	385	417
W_X	464	486	470	500

the pentagon-edge to pentagon-diameter hopping gives a contribution $\propto -4tu$ which is relatively large and of opposite sign. At the $(rr+rr)$ contact, this pentagon-edge to pentagon-diameter contribution proportional to $4rw$ is relatively small and positive. At the $(ss+ss)$ contact, the negative contribution proportional to $-2ss$ from diagonal hops is largly canceled by the contribution proportional to $4sq$ from the pentagon-edge to pentagon-diameter hopping. Finally, at the $(rt+rt)$ contact, the numerical increase due to diagonal hopping proportional to $-2rt$ is largely canceled by the contribution proportional to $2ru$.

In order to obtain the results given in the last two columns of Table II, which present fits to the bands shown in Figs. 4 and 5, we first need to understand the dispersion given by the single-MO Hamiltonian (20).

When the Block vector is along one of the three ΓX lines [e.g., from (0,0,0) to $(2,0,0)\pi/a$], or along one of the three XWX lines [e.g., from $(2,0,0)\pi/a$ to $(2,1,0)\pi/a$ to $(2,2,0)\pi/a$], the off-diagonal Hamiltonian matrix elements vanish and we obtain three bands with cosine dispersion. The bands are degenerate at Γ and reach extrema at the X point. The energy at Γ is $4V_{\|}(rr) - 4V_{\|}(ss) + 4V_{\|}(tt)$ (degeneracy=3).

At X $(2,0,0)\pi/a$, the three energies and corresponding wave functions are $-4V_{\|}(rr)-4V_{\|}(ss)-4V_{\|}(tt)$ and $|X\rangle$, $-4V_{\|}(rr)+4V_{\|}(ss)+4V_{\|}(tt)$ and $|Y\rangle$, and $4V_{\|}(rr)+4V_{\|}(ss)-4V_{\|}(tt)$ and $|Z\rangle$. The bandwidth at X is thus

$$W_X = 8V_{\|}(rr) + 8V_{\|}(ss), \tag{23}$$

and the sum of the energies at Γ and the three X points is zero.

Since W is at the midpoint between two X points and since the bands have cosine dispersion along XWX, the three energies at W are just the averages of the three energies at X and, hence, equal $-4V_{\|}(rr)$, $-4V_{\|}(tt)$, and $4V_{\|}(ss)$. Note that *each* of the three bands along XWX is *not* symmetric around W so that along one XW line the two upper bands cross, and along another the two lower bands cross.

At the L point $(1,1,1)\pi/a$ the energies are seen to be $-4V_{\|}(rt)$ (degeneracy=2) and $8V_{\|}(rt)$, with zero average.

With the Bloch vector along ΓKX (e.g., in the [110] direction), one band ($|Z\rangle$) is pure, but the two others hybridize strongly in the interior of the zone and the corresponding anomalies are clearly seen in Figs. 4 and 5.

In order to fit a given conduction-band structure by hand to this single-MO model, the simplest choice would be first to go to the L point and obtain the conduction-band zero (center of gravity) as the energy which is one-third from the bottom and two-thirds from the top, and to obtain $4V_{\|}(rt)$ as one-third the L bandwidth. The remaining three MO hopping integrals might then be obtained as the energies at W, measured from the conduction-band zero and with appropriate signs. Except for obtaining $12V_{\|}(rt)$ as the bandwidth at L, this procedure is, however, inaccurate because it involves small energy differences and because the model Hamiltonian is not exact; it neglects the interaction with other MO bands. A satisfactory procedure is to use the four energies at Γ and X to find the remaining three coefficients and the center of gravity. Specifically, if we measure the energies with respect to the energy at Γ and if we number the bands at X in order of increasing energy, the result is $16V_{\|}(rr) = E_3 - E_2 - E_1$, $16V_{\|}(ss) = E_3 + E_2 - E_1$, $16V_{\|}(tt) = -E_3 + E_2 - E_1$, and, for the center of gravity, $\langle E\rangle = (E_3 + E_2 + E_1)/4$.

The third column in Table II gives MO-hopping integrals fitted by the above-mentioned procedure to the TB band structure calculated in the radial-AO approximation and shown in Fig. 4. Apart from being perfect at Γ and X, this fit deviates by merely 10 meV at L, and a bit more at W. This TB calculation employed the same AO-hopping integrals given by (13) and (14) as used in the first two columns of the table, but it included all 60 radial AO's rather than just the three LUMO's. The facts that the fit is so good and that the coefficients just differ slightly from the ones obtained using the single-MO approximation, indicates that this approximation is sound for the unidirectional structure, even at the fairly small lattice constant chosen.

The *ab initio* conduction-band structure of RbC_{60} shown in Fig. 5 is very similar to the TB band structure of C_{60} shown in Fig. 4 and the fit to the LDA-LMTO bands is of the same good quality as the fit to the TB bands. From the coefficients given in the last column of Table II we see that the increase of bandwidth W_X is mainly due to the increase of the hopping integral $V_{\|}(rr)$. The actual width of the LDA band is 517 meV rather than W_X=500 meV because the top of the band occurs at the L point.

In Figs. 6, 7, and 8 we show the densities of states for the conduction band calculated, respectively, in the single-MO approximation with converged hopping integrals, with the TB method in the radial-AO approximation (Fig. 4), and with the LMTO method in the LDA for RbC_{60} (Fig. 5). The similarity of Fig. 6, 7, and 8 demonstrates the quality of the radial-AO and the single-MO approximations; the most visible deviations are caused by the cruder Brillouin-zone integration used in Fig. 7. All figures show that in the unidirectional structure, the two lowest subbands are fairly well separated from the uppermost subband with the deep valley between the two peaks being centered approximately at the upper-band crossing along XW. The value of the density of states at the Fermi level corresponding to a doping of three electrons is about 15 states per eV per molecule and for both spins.

A measure of the bandwidth which is easy to calculate in TB theory, even for complicated structures, is

$$W \equiv \sqrt{12\,\langle\,(E-\langle E\rangle)^2\,\rangle}, \tag{24}$$

which would be the exact bandwidth if the density of states were rectangular. In the single-MO approximation, $\langle E\rangle = 0$ and the second energy moment per state may be evaluated as

$$\langle E^2 \rangle = \tfrac{1}{3} \sum_{M'} \sum_{M} \sum_{N=1,12} |\langle M'0|H|MN\rangle|^2, \tag{25}$$

where N runs over the nearest-molecule neighbors. For the unidirectional structure we obtain

$$\langle E^2 \rangle = 4[\, V_{\parallel}(rr)^2 + V_{\parallel}(ss)^2 + V_{\parallel}(tt)^2 + 2V_{\parallel}(rt)^2 \,], \tag{26}$$

where the contributions from the $(sr\text{-}sr)$ and $(st\text{-}st)$ contacts vanish, as we have noted before. Using the MO-hopping integrals listed in Table II, we obtain the effective bandwidths W listed at the bottom of the table. Only within the single-MO approximation is this procedure exact. For the radial-AO bands shown in Fig. 4, for instance, a measure of the importance of MO mixing and, hence, of the quality of the fit, is the difference between the 385 meV given in the table and the correct value of 405 meV, obtained from (24) by using the energy bands and performing the averages over the Brillouin zone.

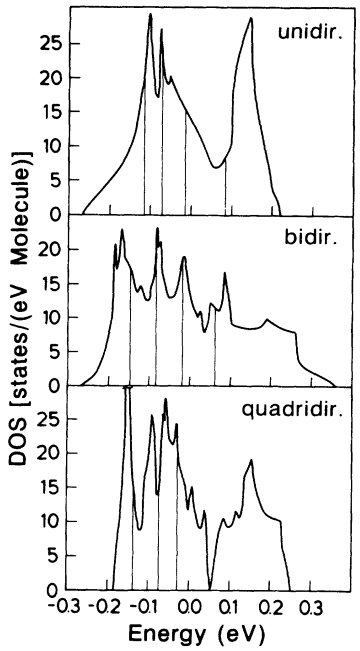

FIG. 6. Conduction-band density of states (DOS) for both spins and per molecule for C_{60} in the unidirectional, bidirectional, and quadridirectional structures with a=14.1 Å. The calculations were performed in the single-MO approximation using the Hamiltonians (20), (28), and (36) with the converged MO-hopping integrals listed in Tables II, III, and IV. The zero of energy is at the center of gravity and the vertical lines indicate the Fermi levels for dopings of one, two, three, and four electrons per molecule. The Brillouin-zone integrations were performed with the tetrahedron method using 1030 (uni), 726 (bi), and 451 (quadri) irreducible points. Scaling to other lattice constants as explained in Sec. IV C.

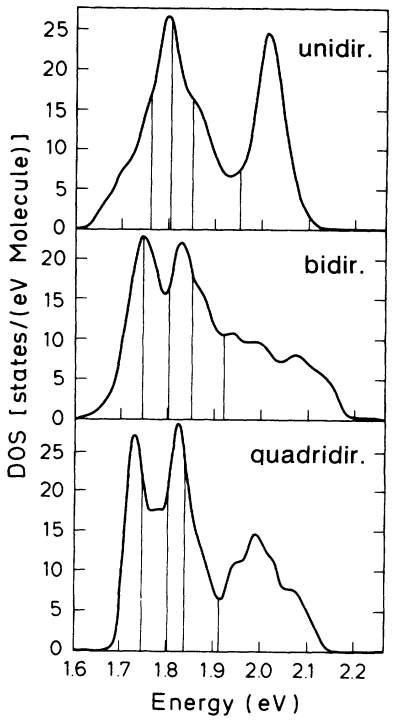

FIG. 7. Same as Fig. 6, except that the bands were calculated with the TB method in the radial-AO approximation and are shown in Figs. 4, 9, and 10. The Brillouin-zone integrations were performed by sampling over 125 points in the irreducible 1/8th of the sc zone and smoothening with a Gaussian proportional to $\exp[-(E - E_0)/20\ \text{meV}]^2$. The zero of energy is at the top of the valence band in the unidirectional structure.

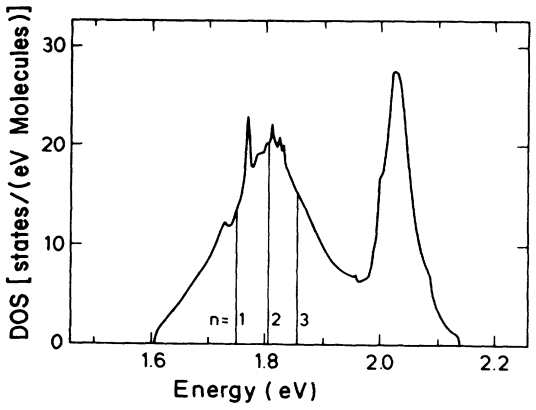

FIG. 8. LDA-LMTO conduction-band density of states for both spins and per molecule for RbC_{60} in the unidirectional structure with a=14.1 Å. The bands are shown in Fig. 5. The Fermi level is labeled n=1 and the levels corresponding to doping with two and three electrons are shown, too. The Brillouin-zone integration was performed with the tetrahedron method using 396 irreducible points. Scaling to other lattice constants as explained in Sec. IV C.

C. Bidirectional conduction band

In the bidirectional crystal, the molecular orientations alternate between y and x when we proceed from one (001) layer to the next. For a given molecule, therefore, one-third of the neighbors have parallel orientation, like in the unidirectional structure, and two-thirds have perpendicular orientation. Now, we have seen in Eq. (15) that the AO nearest-neighbor integral for perpendicular orientation is 10% larger than for the parallel orientation (for the same lattice constant) and we therefore expect the conduction band in the bidirectional structure to be about 6.7% wider. Before dealing with the intricacies of the dispersion in this structure with two molecules per cell, let us now investigate this question of the bandwidth in slightly more detail by using the single-MO approximation and the second-moment procedure (25).

We easily find that the second moment is given by the same expression (26) as for the unidirectional structure, but with the substitutions

$$V_{\parallel}(c_1c_2)^2 \rightarrow \tfrac{1}{3}V_{\parallel}(c_1c_2)^2 + \tfrac{2}{3}V_{\perp}(c_1c_2)^2. \qquad (27)$$

In the nearest-neighbor approximation our expectation therefore holds with good accuracy.

The converged MO-hopping integrals for the perpendicular orientation [defined in Eq. (22)] are listed in Table III where, at the bottom, we give the effective bandwidths obtained using these hopping integrals together with those of Table II for the parallel orientation. The results are that long-range hopping is relatively important in the bidirectional structure and that it increases the effective bandwidth W from the nearest-neighbor result, which is 6.7% larger, to being 20% larger than in the unidirectional structure. The main cause for this increase is that whereas longer-range hopping decreased $V_{\parallel}(tt)$, it increases $V_{\perp}(tt)$ and it significantly increases $V_{\perp}(ss)$. The reason is that with perpendicular orientation, pentagons face pentagons (rather than hexagons) and the dominant contribution to the long-range hopping is now from pentagon diameter to pentagon diameter (rather than from edge to diameter). As seen in Fig. 1, this contribution is particularly strong for the $(ss+ss)$ contact, where the pentagon diameter has the large LUMO amplitude q.

The densities of states in Fig. 6 for the converged single-MO approximation clearly exhibit this 20% increase of effective bandwidth, and corresponding decrease of state density, when going from the unidirectional to the bidirectional structure. If we compare the widths between the actual band edges, the increase is even 30%, but this is hardly relevant because, in both structures, these widths are strongly influenced by tails at the top of the band. On the other hand, for an occupancy of three electrons per molecule, the Fermi level falls at a density-of-states peak in the bidirectional structure. For the relevant occupancy, therefore, the density of states is about the same [17 st./(mol eV)] for the unidirectional and bidirectional structures. Figure 9 shows the conduction band for the bidirectional structure at the standard lattice constant, now calculated with the TB method in the radial-AO approximation. This band is noticeably broader than the unidirectional band, and its high-energy tail even overlaps the next higher band. The density of states for the six lowest radial-AO bands is shown in the middle of Fig. 7. It resembles the single-MO result, but there is a slight shift of weight from the high-energy to the low-energy part.

Another important difference between the densities of states for the two structures is that the low-energy peak is split (into two or three) in the bidirectional structure, and this causes the conduction-band energy to be lower than for the unidirectional structure when the occupancy is about three electrons. This contribution to the orientational energy in favor of the bidirectional structure for the doped compounds should be added to the contributions from MO mixing considered in Ref. 15.

We now discuss the dispersion in detail by deriving the 6×6 band Hamiltonian in the single-MO approximation and diagonalizing it in k-space planes, lines, or points of

TABLE III. Additional t_{1u}-hopping integrals and derived effective W and real W_{Γ} bandwidths for the bidirectional structure and a=14.10 Å. Otherwise like Table II.

	Single MO		Radial AO
(meV)	Nearest neighbor	Conv.	Fig. 9
$4V_{\perp}(rr)$	156	186	150
$4V_{\perp}(ss)$	99	164	170
$4V_{\perp}(tt)$	71	109	105
$4V_{\perp}(rt)$	105	93	95
W	416	484	465
W_{Γ}	611	627	635

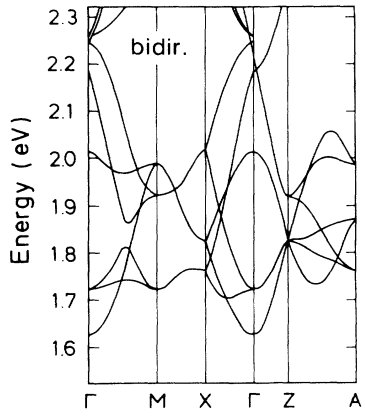

FIG. 9. C_{60} conduction band in the bidirectional structure with a=14.1 Å calculated in the radial-AO TB approximation. The primitive tetragonal Brillouin zone is a box centered at Γ (0,0,0) with edge centers at M $(2,0,0)\pi/a$, face centers at X $(1,1,0)\pi/a$ and Z $(0,0,1)\pi/a$, and with corners at A $(2,0,1)\pi/a$. The X point at $(0,0,2)\pi/a$ in the fcc Brillouin zone is now folded into Γ. The Fermi levels for dopings of one, two, three, and four electrons per molecule are, respectively, 1.75, 1.80, 1.85, and 1.92 eV. The density of states is shown in Fig. 7. Otherwise, as in Fig. 4.

high symmetry.

The translation cell is primitive tetragonal and contains two equivalent molecules, one with y orientation at the origin and one with x orientation at $(0,1,1)a/2$. We shall use a notation according to which $|Mx\rangle$ and $|My\rangle$ are Bloch sums of $|M\rangle$ LUMO's on the x and y sublattices, respectively. Since the group of rotation translations which take any molecule into any other is not commutative (Abelian), it is not possible with suitable redefinition of the Bloch sums to reduce the band-structure problem to one involving just a *single* molecule.

Due to the inversion and mirror symmetries of the LUMO partners (see Figs. 1 and 2), the Hamiltonian matrix can be written in the following form:

$$H = A\cos(k_x a/2)\cos(k_y a/2) + B\cos(k_y a/2)\cos(k_z a/2) + C\cos(k_z a/2)\cos(k_x a/2)$$
$$+D\sin(k_x a/2)\sin(k_y a/2) + E\sin(k_y a/2)\sin(k_z a/2) + F\sin(k_z a/2)\sin(k_x a/2), \tag{28}$$

where A through F are sparse 6×6 matrices which we shall specify below. It is obvious that A and D provide the hopping *in* the (001) planes and therefore will be given by $V_{\|}$ integrals while B, C, E, and F provide hopping between planes and therefore are given by $V_{\perp}$ integrals.

It will prove useful to arrange the orbitals in the order $|Yy\rangle$, $|Xx\rangle$, $|Xy\rangle$, $|Yx\rangle$, $|Zx\rangle$, and $|Zy\rangle$ because, by virtue of the mirror symmetries, there is no coupling between $|Yy\rangle$ and $|Yx\rangle$, between $|Xx\rangle$ and $|Xy\rangle$, between $|Zy\rangle$ and $|Yy\rangle$, between $|Zx\rangle$ and $|Xx\rangle$, between $|Zy\rangle$ and $|Xy\rangle$, and between $|Zx\rangle$ and $|Yx\rangle$. The matrices A, B, and C are 2×2 block diagonal, with A being strictly diagonal, and B and C giving the coupling. The three 2×2 off-diagonal blocks of the 6×6 matrix are represented by D, E, and F, respectively, and each of them are "diagonal."

The diagonal matrix A now has the following nonzero elements:

$$\begin{aligned}
&\langle Yy|A|Yy\rangle = \langle Yx|A|Yx\rangle = 4V_{\|}(rr),\\
&\langle Xx|A|Xx\rangle = \langle Xy|A|Xy\rangle = 4V_{\|}(tt),\\
&\langle Zx|A|Zx\rangle = \langle Zy|A|Zy\rangle = -4V_{\|}(ss).
\end{aligned} \tag{29}$$

B and C provide the coupling in the 2×2 diagonal blocks,

$$\begin{aligned}
\langle Yy|B|Xx\rangle &= -\langle Xy|C|Yx\rangle = -\langle Zx|C|Zy\rangle\\
&= -\langle Zx|B|Zy\rangle = 4V_{\perp}(rt),\\
\langle Yy|C|Xx\rangle &= -\langle Xy|B|Yx\rangle = 4V_{\perp}(ss).
\end{aligned} \tag{30}$$

Finally,

$$\begin{aligned}
&\langle Yy|D|Xy\rangle = -\langle Xx|D|Yx\rangle = 4V_{\|}(rt),\\
&\langle Yy|E|Zx\rangle = \langle Yx|F|Zy\rangle = -4V_{\perp}(tt),\\
&\langle Xx|E|Zy\rangle = -\langle Xy|F|Zx\rangle = 4V_{\perp}(rr).
\end{aligned} \tag{31}$$

All matrix elements not mentioned in (29)–(31), except the transposed ones, vanish.

When the sine coefficients of E and F in (28) vanish, i.e., when the Bloch vector is in the $k_z=0$ plane, along the k_z axis (ΓZ), or along the line MA parallel herewith, there is no coupling between the two $|Z\rangle$ MO's and the four $|X\rangle$ and $|Y\rangle$ MO's. The corresponding grouping of the six bands in 2 plus 4 is clearly seen in Fig. 9 along the lines ΓM, MX, $X\Gamma$, and ΓZ.

We first consider the two $|Z\rangle$ bands, which are given by the corresponding block of the A, B, and C terms. Since the A block is degenerate, the dispersion of the $|Z\rangle$ bands is simply

$$E = -4V_{\|}(ss)\cos(k_x a/2)\cos(k_y a/2)$$
$$\pm 4V_{\perp}(rt)\,[\cos(k_x a/2) + \cos(k_y a/2)]\cos(k_z a/2), \tag{32}$$

so that the energies are $-4V_{\|}(ss)\pm8V_{\perp}(rt)$ at Γ, $4V_{\|}(ss)$ at M, 0 at X, $-4V_{\|}(ss)$ at Z, and $4V_{\|}(ss)$ again at A. The lowest level at Γ marks the bottom of the band. In the figure, the $|Z\rangle$ levels are the highest at M and A, and these levels coincide with the highest level at W in the unidirectional structure.

We then consider the four $|X\rangle$ and $|Y\rangle$ bands in the ΓMX plane, along ΓZ, and along MA. Along the two latter lines and along ΓM, all sine factors in (28), including the coefficient of D, vanish, so that the $|Yy\rangle$ and $|Xx\rangle$ bands do not mix with the $|Xy\rangle$ and $|Yx\rangle$ bands. The energies at Γ and M are doubly degenerate and equal,

$$E = 2V_{\|}(rr) + 2V_{\|}(tt)$$
$$\pm\sqrt{[2V_{\|}(rr) - 2V_{\|}(tt)]^2 + [4V_{\perp}(rt) + \nu 4V_{\perp}(ss)]^2}, \tag{33}$$

where $\nu=1$ for Γ and -1 for M. The highest level at Γ marks the top of the band. (In the figure this level is the one at 2.25 eV.) At the midpoint between Γ and M, only the B term of the Hamiltonian is nonzero and the energies are simply $\pm4V_{\perp}(ss)$ and $\pm4V_{\perp}(rt)$. At Z the doubly degenerate energies are $4V_{\|}(rr)$ and $4V_{\|}(tt)$, and at A they are $-4V_{\|}(rr)$ and $-4V_{\|}(tt)$.

At the X point the only nonvanishing term of the Hamiltonian is D, so that the three doubly degenerate energies are $\pm4V_{\|}(rt)$ and 0, which is $|Z\rangle$-like as mentioned above. Finally, at the midpoint between Z and A, only the F term survives so that the six energies are $\pm4V_{\perp}(rr)$, $\pm4V_{\perp}(tt)$, and 0. The latter energy is dou-

bly degenerate and marks the crossing along ZA of the cosinelike, pure $|Yy\rangle$ and $|Xx\rangle$ bands.

The above-mentioned description of the conduction-band structure gives the basis for understanding how each MO-hopping integral influences the dispersion. In order to *fit*, for instance, the radial-AO band in Fig. 9 to this t_{1u} model, the following procedure is simple and reasonably accurate: $8V_{\perp}(rr)$ and $8V_{\perp}(tt)$ are obtained as energy differences at the ZA midpoint, $16V_{\perp}(rt)$ as the splitting of the $|Z\rangle$ bands at the Γ point, and $8V_{\perp}(ss)$ as the largest splitting of the $(|X\rangle, |Y\rangle)$ bands at the ΓM midpoint. $8V_{\parallel}(rt)$ is obtained as the bandwidth at X and, finally, differences between levels at Z and A give $8V_{\parallel}(rr)$, $8V_{\parallel}(rr)$, and $8V_{\parallel}(tt)$. The center of gravity may be obtained at X, or at the ZA midpoint, or better, as a suitable average.

The result of this procedure applied to the radial-AO band in Fig. 9 is included in Table III as regards the hopping between perpendicular molecules. The values are quite close to those calculated properly using the single-MO approximation, except maybe $V_{\perp}(rr)$, which is a bit low. The parameters for hopping between parallel molecules should equal those fitted to the unidirectional radial-AO band and given in Table II. With those values in Eq. (27) we obtain an effective bandwidth of W=465 meV for the bidirectional structure. This number is given at the bottom line in Table III. Direct numerical calculation for the six lowest bands of Fig. 9 yields 445 meV.

The integrals for hopping between parallel molecules fitted directly to the bidirectional radial-AO band structure are $4V_{\parallel}(rr)$=80, $4V_{\parallel}(ss)$=75, $4V_{\parallel}(tt) = -25$, and $4V_{\parallel}(rt)$=125 meV. The value for $4V_{\parallel}(rr)$ is almost half the one obtained from fitting the unidirectional band structure, but the other values are more reasonable. Inserting these values in Eq. (27) we obtain an effective bandwidth of W=455 meV which is closer to the 445 meV calculated by Brillouin-zone integration; this indicates that the fit has, in fact, been improved. The factor-two discrepancy for $4V_{\parallel}(rr)$ presumably arises because the highest level at Z, which is used for determining this parameter, has been pushed down considerably by hybridization with the above-lying MO band. This effect is seen most clearly at Γ where the lowest level of the higher MO-band lies below the highest doubly degenerate level of the t_{1u} band; since these levels do not seem to mix at Γ this does, however, not influence our parameters (but the directly calculated effective bandwidth, of course). Along ΓM the two nearly crossing bands are clearly influenced by the higher MO band: in the single-MO theory their distance at the ΓM midpoint equals half the splitting between the $|Z\rangle$ levels at Γ [$=16V_{\perp}(rt)/2$=210 meV], but in reality it is only 50 meV. Finally, at the X point the $|Z\rangle$ energy should be the average of the $(|X\rangle, |Y\rangle)$ energies, which it is clearly not.

For the bidirectional radial-AO band at a=14.1 Å, MO mixing is therefore not negligible. Nevertheless, the densities of states in Figs. 6 and 7 calculated in, respectively, the single-MO and the radial-AO approximations without fitting the results of the latter to the former, are in reasonably good agreement. Besides, at the lattice constants $a \approx$14.25–14.45 Å where the bidirectional structure is relevant, the importance of MO mixing should be reduced.

Since the bidirectional structure is presumably a good approximation to the local structure of the real, doped superconducting compounds, it is important to estimate the hopping integrals for its conduction band as well as possible. For lack of a real LDA calculation, but in view of the good agreement found for the unidirectional structure with the radial-AO approximation, we recommend using the radial-AO values from Tables I and II.

D. Quadridirectional conduction band

The density of states for the quadridirectional structure at the standard lattice constant and calculated in the single-MO approximation is shown at the bottom of Fig. 6. The 12 conduction bands obtained by diagonalizing the 240 × 240 radial-AO Hamiltonian are shown in Fig. 10 and their state density is at the bottom of Fig. 7. Apart from the difference in resolution, the densities of states resulting from the single-MO and the radial-AO approximations are for practical purposes identical, and the same holds for the bands.

The bands roughly group into three bundles with four bands in each and the density of states has three corresponding peaks, each of which can hold two electrons per molecule. Similar to the unidirectional conduction band, the upper one-third of the quadridirectional band is nearly separated from the lower two-thirds, but the valley is much narrower and the lower two-thirds is relatively more compressed. At the standard lattice constant, the bandwidth W_R is 435 meV which is 90% of the unidirectional bandwidth W_X (and 69% of the bidirectional

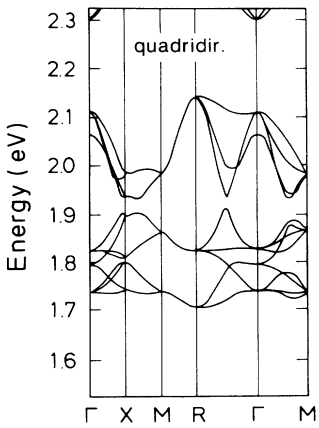

FIG. 10. C_{60} conduction band in the quadridirectional structure (space group $Pa\bar{3}$) with a=14.1 Å calculated in the radial-AO TB approximation. The Brillouin zone is a cube centered at Γ (0,0,0) and with face centers at X $(1,0,0)\pi/a$, edge centers at M $(1,1,0)\pi/a$, and corners at R $(1,1,1)\pi/a$. The Fermi levels for dopings of one, two, three, and four electrons per molecule are, respectively, 1.74, 1.80, 1.84, and 1.91 eV. The density of states is shown in Fig. 7. Otherwise, as in Fig. 4.

bandwidth W_Γ). The effective bandwidth, W=420 meV, is slightly larger than for the unidirectional structure and is, in fact, quite close to the real bandwidth W_R. This reflects the compactness of the quadridirectional conduction band.

That the bandwidths for the quadridirectional and unidirectional structures are about the same for the same lattice constant is not what one would have expected from the reduction of the AO-hopping integrals: according to (15) the latter are reduced by 22% for the nearest AO pair and by 32% for the second-nearest pair. As we shall see, the reason is that for this edge-to-face contact the LUMO-hopping integrals are relatively large due to constructive interference in the sums (22). Like for the perpendicular orientation, this constructive interference extends to beyond first and second-nearest-atom neighbors. This is the same kind of effect which is responsible for the stability of the quadridirectional structure, the only difference being that now the effect works *within* the t_{1u} band. In the following, we shall use the single-MO approximation, first to evaluate the effective bandwidth and then to derive the band Hamiltonian.

The MO-hopping integrals are defined in (22), and for the quadridirectional structure (see Fig. 3) the notation is such that, for instance, $V_\phi(tt+pw)$ describes the hopping from a pentagon diameter with LUMO amplitudes $-t$ and p, to a hexagon edge with LUMO amplitudes $-t$ and w. The first term, tt, refers to the shorter contact distance and the second, pw, to the longer. In the nearest-two-neighbors approximation, therefore,

$$V_\phi(c_1c_2+c_3c_4)=c_1V_\phi c_2+c_3V_{\phi 2}c_4, \tag{34}$$

and in Table I we defined $o\equiv 0$. With the values of V_ϕ and $V_{\phi 2}$ in Eq. (15) and the LUMO coefficients from Eq.(19) we obtain the values for the nine MO-hopping integrals given in the first column of Table IV. By comparison with the converged values given in the second column, the former are in most cases too small.

The second moment may now be obtained from Eq. (25) by summing over the contacts and the LUMO's. The result is simply,

$$\begin{aligned}\langle E^2\rangle \;=\; 4\,[\; & V_\phi(rr+vq)^2+V_\phi(ss+ou)^2+V_\phi(tt+pw)^2+V_\phi(rs+vu)^2+V_\phi(sr+oq)^2\\ & +V_\phi(rt+vw)^2+V_\phi(tr+pq)^2+V_\phi(st+ow)^2+V_\phi(ts+pu)^2\;]. \end{aligned}\tag{35}$$

The effective bandwidths obtained herefrom are given at the bottom of the table and the converged value W=420 meV is in reasonable agreement with the 400 meV obtained by direct calculation using the radial-AO approximation. The point, that in comparison with the unidirectional structure, the increased contact distance is compensated by a better match in the contact region of the c phases, may be illustrated by comparing the second moments calculated from Eqs. (35) and (26) by setting $V_\parallel = V_\phi = V_{\phi 2} = V$ and neglecting all farther hoppings. The results for the effective bandwidths are W_{quadri}=0.609V and W_{uni}=0.526V, that is, the nearest- and second-nearest-neighbor phase effect improves the hopping by about 15%. That, in addition, there is longer-range constructive hopping at this edge-to-face contact may be illustrated by comparing the ratios $W_{\text{conv}}/W_{\text{NN}}$ for the different structures: From Tables II, III, and IV we obtain increases of, respectively, 3%, 16%, and 24% for the unidirectional, bidirectional, and quadridirectional structures.

TABLE IV. t_{1u}-hopping integrals and derived effective W and real W_R bandwidths for the quadridirectional structure and a=14.10 Å. Otherwise like Table II.

(meV)	Single MO Nearest two neighbors	Conv.
$4V_\phi(rr+vq)$	76	77
$4V_\phi(ss+ou)$	36	−20
$4V_\phi(tt+pw)$	40	44
$4V_\phi(rs+vu)$	55	75
$4V_\phi(sr+oq)$	46	67
$4V_\phi(rt+vw)$	42	48
$4V_\phi(tr+pq)$	128	155
$4V_\phi(st+ow)$	31	57
$4V_\phi(ts+pu)$	74	104
W	339	420
W_R	335	435

We now work out the band Hamiltonian. The translation cell is simple cubic and the molecules at (1,1,0)$a/2$, (0,1,1)$a/2$, and (1,0,1)$a/2$ are rotated with respect to the one at (0,0,0) by 180° around the x, y, and z axes, respectively. The molecule at (0,0,0) (Fig. 3) is rotated around the threefold [111] axis by $-\varphi$ with respect to one with y orientation (Fig. 2). As for the bidirectional structure, the group of rotation translations which take a molecule into any other is not commutative and, as a consequence, it is not possible to reduce the band-structure problem to one involving just a single molecule per cell. The Bloch sums are therefore over the four sc sublattices and, in the following, $|M,110\rangle$ denotes such a sum. Here, M refers to a LUMO in the *local* coordinate system. The order of the Bloch orbitals we take as $|X,000\rangle$, $|Y,000\rangle$, ... , $|Z,101\rangle$, and the 12 × 12 Hamiltonian we thus imagine as composed of 3 × 3 blocks. With the help of Fig. 3 and using the symmetries of the t_{1u} partners one may now derive the following expressions.

Since we include hopping only between nearest-neighbor molecules and since we take the LUMO level as the zero of energy, the four *diagonal blocks* of the Hamiltonian *vanish*. For the off-diagonal blocks we have

$$\langle 000|H|110\rangle = \langle 011|H|101\rangle^{\dagger} = S\cos[(k_x+k_y)a/2] + S^{\dagger}\cos[(k_x-k_y)a/2],$$

$$\langle 000|H|101\rangle = \langle 110|H|011\rangle^{\dagger} = U\cos[(k_z+k_x)a/2] + U^{\dagger}\cos[(k_z-k_x)a/2], \quad (36)$$

$$\langle 000|H|011\rangle = \langle 110|H|101\rangle = T\cos[(k_y+k_z)a/2] + T^{\dagger}\cos[(k_y-k_z)a/2].$$

Here, S, T, U, $\langle 011|H|101\rangle$, etc. are meant to be 3×3 matrices with elements $\langle L|S|M\rangle$, and this implies that $\langle L|\langle 011|H|101\rangle^{\dagger}|M\rangle = \langle M|\langle 011|H|101\rangle|L\rangle$, and of course not $\langle M|\langle 101|H|011\rangle|L\rangle$.

The matrices S, T, and U are related through

$$\langle L-1|S|M-1\rangle = \langle L|T|M\rangle = \langle L+1|U|M+1\rangle. \quad (37)$$

Hence, of the 144 coefficients in the Hamiltonian there are only 9 independent ones and these are given by the MO-hopping integrals

$$U = 2\begin{pmatrix} -V_\phi(rr+vq) & V_\phi(rs+vu) & -V_\phi(rt+vw) \\ V_\phi(sr+oq) & -V_\phi(ss+ou) & V_\phi(st+ow) \\ V_\phi(tr+pq) & -V_\phi(ts+pu) & V_\phi(tt+pw) \end{pmatrix}. \quad (38)$$

The band edges are at the R point $(1,1,1)\pi/a$ and, here, where each of the three bundles are degenerate, we are able to diagonalize the Hamiltonian analytically. The cosines in (36) are either plus or minus unity so that the Hamiltonian is given in terms of $S^{\dagger}-S$, $T^{\dagger}-T$, and $U^{\dagger}-U$. Therefore only the following three combinations of hopping integrals enter:

$$2\,[V_\phi(rs+vu) - V_\phi(sr+oq)] \equiv 4V_\phi(rs), \quad (39)$$

which is a small difference, and

$$2\,[V_\phi(rt+vw) + V_\phi(tr+pq)] \equiv 4V_\phi(rt),$$
$$2\,[V_\phi(st+ow) + V_\phi(ts+pu)] \equiv 4V_\phi(st). \quad (40)$$

The bottom of the band now has the energy

$$E_1 = -4V_\phi(rs) - 4V_\phi(rt) - 4V_\phi(st), \quad (41)$$

and the two remaining energies are

$$E_{3/2} = -\tfrac{1}{2}E_1 \pm (12\{V_\phi(rs)^2 + V_\phi(rt)^2 + V_\phi(st)^2 + [V_\phi(rs)-V_\phi(st)]^2 + [V_\phi(rt)-V_\phi(rs)]^2 + [V_\phi(st)-V_\phi(rt)]^2\})^{1/2}. \quad (42)$$

E_3 is the top of the band so that $W_R = E_3 - E_1$. The center of gravity at R is seen to equal the center of gravity of the entire t_{1u} band. Using the MO-hopping integrals from Table IV we obtain the following R point energies: -186, -63, and 249 meV. Their differences of 123 and 312 meV compare well with the 117 and 316 meV obtained from the TB calculation in the radial-AO approximation (Fig. 10).

IV. LDA LMTO-ASA CALCULATIONS

For the numerical LDA calculations we used the linear-muffin-tin-orbitals method (LMTO) in the atomic-spheres approximation[17] (ASA) due to its efficiency in treating solids with many atoms per cell. For C_{60} this efficiency is somewhat offset by the necessity to use interstitial spheres in addition to atomic spheres. Interstitial spheres must be small, unless they are at sites of high symmetry. Moreover, the sum of the sphere volumes should equal the cell volume and the sphere overlaps should be small. Hence, the choice of spheres requires care in order that the details of the bands and their dependence on the lattice constant be accurate. We used a total of 134 spheres: The shell of 60 carbon spheres (radius s=0.6b) was given an inner and an outer "skin" of interstitial spheres, each consisting of 12 spheres on top of pentagons, plus 20 on top of hexagons (s_i=0.6b, s_o=0.7b). In addition, we used a large sphere (s=1.38b) at the center of the molecule. Between the molecules, we placed large spheres at all corners and edges of the fcc Wigner-Seitz cell, specifically, at $(0,0,1)a/2$ and at $(1,1,2)a/6$. Of the former octahedral spheres there is one per molecule; its radius was chosen as $s = (a/2) + (3\tau+1)b/2$. Of the latter edge spheres there are eight per molecule and we chose their radius such that the sum of all sphere volumes equals the cell volume.

The basis set consisted of the s- and p-LMTO's on the carbon and octahedral sites, plus the s-LMTO's on all remaining sites. This set of 317 LMTO's per cell was constructed through downfolding of the set having s, p, and d LMTO's on all sites (1206 LMTO's per molecule). The downfolding was performed in such a way that the tail of each LMTO in the 317 set satisfies the radial Schrödinger equation for all the (1206−317) downfolded partial waves at *one* energy, the center of gravity of the occupied part of the projected state density.[17] Charge-self-consistency was obtained with 18 irreducible k points and the density of states for the self-consistent potential was calculated using the full-zone tetrahedron method with 396 irreducible k points.

A. Comparison with photoemission and inverse photoemission experiments for C_{60}

The LDA band structure for unidirectional fcc C_{60} with *equal* bond lengths ($b_h = b_p = b$) near the HOMO-(highest occupied molecular orbital) LUMO gap is shown in the left-most panel of Fig. 11. We used a=14.10 Å which is intermediate between the values measured at 11 K (14.04 Å) and at 300 K (14.17 Å).[4] The valence bands start 19 eV below the top of the valence band in agreement with photoemission data[18] and other calculations.[12,18,14] The top of the bonding σ bands is at −4 eV and all other bands in Fig.11 are π like.

Recent photoemission data[18] for solid C_{60} at room temperature show well-defined peaks from individual MO bands whose parities were deduced: The peak derived from the HOMO is approximately 0.7 eV wide and this MO is odd. At 1.3 eV below the HOMO there is a 1-eV-wide peak of even character and 3.6 eV below, a 1.4-eV-wide peak of mixed character. This agrees with our h_u, g_g, h_g, g_u and following bands, except that our h_g band may lie 0.2 eV too low and our g_u band 0.3 eV too high. The calculated, dispersional bandwidths are comparable to the experimental ones. Experiments show, however, a substantial level width also for free molecules, which presumably is due to vibrational satellites.[20] For solids one may therefore expect a substantial contribution to the bandwidth from phonon satellides, while polaron effects may reduce the dispersional width. Inverse photoemission[19] gives peaks 1.2 and 2.1 eV above the center of the LUMO. This confirms our t_{1u}-t_{1g} separation but indicates that our h_g or t_{2u} band lies 0.6 eV too high.

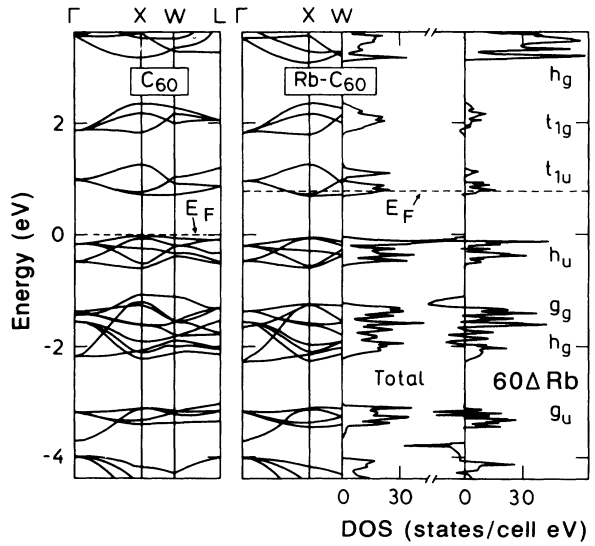

FIG. 11. LDA-LMTO band structures of C_{60} and RbC_{60} in the unidirectional fcc structure and for the same lattice constant, a=14.1 Å. On the right-hand side we show the total density of states (both spins) for RbC_{60} and 60 times the Rb-induced state density projected onto the octahedral sphere. This calculation used equal bond lengths.

The experimental HOMO-LUMO gap is about 3.5 eV (Ref. 21) which is considerably larger than the value of 0.8 eV for the direct gap at X calculated for equal bond lengths. With proper bond lengths (4) the gap widens to the value 1.6 eV (seen in Figs. 4, 5, 7, and 8). That the gap is still too small is consistent with the well-known tendency of the LDA to underestimate gaps in nonmetals. For the highly doped system bcc K_6C_{60}, the experimental separation between the *centers* of the t_{1u} and the h_u bands is reduced to 1.6 eV (Ref. 8) and, hence, only slightly larger than our LDA result with equal bond length. Since the t_{1u} band is now completely occupied, our result is consistent with the experience that the LDA describes occupied states rather accurately, even for nonmetals and that the occupation of the t_{1u} band reduces the difference in bond lengths. The earlier LDA linear combination of atomic orbitals (LCAO) calculation for C_{60} of Saito and Oshiyama[14] gave a direct X gap of 1.5 eV whereas the recent LDA pseudopotential plane-wave calculation of Martins, Troullier, and Schabel[22] and Weaver *et al.* and Benning *et al.*[18] has a gap of less than 1 eV. The most recent LDA LCAO calculation for K_3C_{60} by Erwin and Pickett[23] has a gap of 1.1 eV.

B. Alkali-metal doping

On the right-hand side of Fig. 11 we show the bands near the Fermi level and the density of states for RbC_{60}. For ease of comparison, the same lattice constant, a=14.1 Å, was chosen as for C_{60}. The bands are essentially unaffected by the presence of Rb at the octahedral position and the extra electron is seen to enter the t_{1u} band. There can thus be no extra band below it. The LDA-LMTO conduction band for unidirectional RbC_{60} was shown in Figs. 5 and 8 and was discussed in detail in Sec. III B. In particular, it was shown that this LDA conduction band can be fitted well by the t_{1u} TB model without accounting explicitly for hybridization with alkali-metal orbitals (Table II).

This is consistent with the facts that the energy E_s of the alkali-metal valence s level above that of the t_{1u} level is several eV, and that the interaction $\langle s,\alpha|H|M\rangle$ of the alkali-metal s orbital at site α with the t_{1u} orbital, and with all lower orbitals, is too weak to create a split-off band. In Fig. 12 we show the valence-electron density in the yz plane containing Rb at the octahedral sites. Rb is seen to be almost completely ionized. In the right-most panel of Fig. 11 we show the density of states projected onto the octahedral sphere for RbC_{60}, minus the same function for C_{60}. The hybridization of the t_{1u} (and of the t_{1g}) band is seen to be particularly small, and the h_u, g_g, and h_g bands are merely pushed down slightly.

The reason why the t_{1u} band hardly interacts with alkali-metal atoms at the octahedral sites is that the symmetry of, e.g., the $|Z\rangle$ orbital in Fig. 1 is such that it can only couple to an s orbital at an octahedral site on the z axis, but not to one on the x or the y axis; moreover, the amplitude of $|Z\rangle$ is relatively small at the top hexagon edge along the z axis. Quantitatively, and in the single-MO and nearest-neighbor approximations, the relative octahedral A s character of the LUMO is

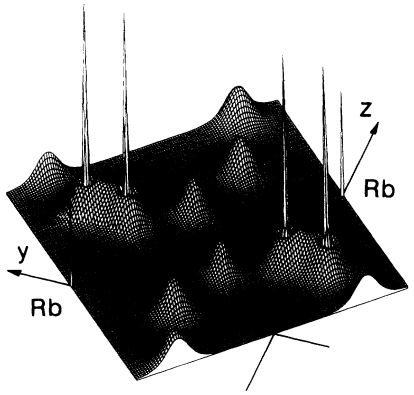

FIG. 12. Valence charge-density in the yz plane (see Fig. 2) for RbC_{60} in the fcc unidirectional structure. The plane passes through the Rb octahedral sites and, for each of two neighboring molecules, it contains a top hexagon edge and passes between two contact atoms plus the midpoint of another top hexagon edge. The Rb $5s$ electron is seen to be transferred to the C_{60} molecule.

$$\Delta n/n = \sum_{\alpha} |\langle s,\alpha|H|Z\rangle|^2/E_s^2$$
$$= (V_{\rm oct}/E_s)^2 \sum_{\alpha}\left|\sum_{\beta} c_{\alpha\beta}\right|^2 = (V_{\rm oct}/E_s)^2 2(2v)^2$$
$$= (V_{\rm oct}/E_s)^2 2/[5(9\tau+10)] \approx 0.016(V_{\rm oct}/E_s)^2. \quad (43)$$

Here, α runs over the six octahedral sites and, for each of these, β runs over the two nearest C neighbors, i.e., those forming the neighboring top-hexagon edge. $c_{\alpha\beta}$ are the LUMO c coefficients given in Fig. 1 and $V_{\rm oct}$ is the integral for hopping from the alkali-metal s orbital to the nearest-neighbor radial carbon AO. From the LDA calculation we find that the relative octahedral A s character of the LUMO is less than 10^{-3} and, hence, that $V_{\rm oct} < E_s/4$.

In A_3C_{60} there are alkali-metal atoms also at the tetrahedral sites $(1,1,1)a/4$, i.e., on top of the hexagons marked by triangles in Fig. 2. Also the electrons from these donors enter an essentially rigid t_{1u} band, because the hybridization between the LUMO and tetrahedral s orbitals is small. The above-mentioned tight-binding expression, with α running over the eight tetrahedral sites and β running over the six C atoms of the nearest hexagon, now yields

$$\Delta n/n = (V_{\rm tet}/E_s)^2 8(-q+r-s-t+u+w)^2$$
$$= (V_{\rm tet}/E_s)^2 8\tau^2/[5(9\tau+10)] \approx 0.171(V_{\rm tet}/E_s)^2, \quad (44)$$

for the relative tetrahedral A s character of the LUMO in A_3C_{60}. Since the nearest-neighbor A-C distance is 3.82 Å for the octahedral site and 3.33 Å for the tetrahedral site (for a=14.4 Å), $V_{\rm tet}/V_{\rm oct} \simeq 1.32$ if we take the sp hopping integral to scale like the inverse distance squared. As a result, the LUMO contains about 20 times more tetrahedral than octahedral A s character in A_3C_{60}; nevertheless, the total hybridization is small. These estimates are seen to be unchanged for the bidirectional structure, which presumably is the relevant one for alkali-metal-doped C_{60}.

For the quadridirectional structure (Fig. 3), the nearest-neighbor TB estimate of the relative s character in the LUMO of octahedral alkali-metal atoms is

$$\Delta n/n = (V_{\rm oct}/E_s)^2 2[(p+u)^2 + q^2 + (w-v)^2]$$
$$\approx 0.278(V_{\rm oct}/E_s)^2. \quad (45)$$

Since the distance from the octahedral site to this pentagon edge is slightly larger than to the top hexagon edge in the unidirectional and bidirectional structures, $V_{\rm oct}$ is now somewhat smaller. For the quadridirectional structure, there is therefore about 15 times more octahedral A s character in the LUMO than for the unidirectional and bidirectional structures. The by-mixing is thus a few percent. At the tetrahedral site there is considerably less room for dopants in the quadridirectional structure than in the two other structures and it is unlikely that large alkali-metal dopants enter this site. We thus consider it possible that the quadridirectional structure of pure C_{60} is retained for low doping levels, but not for $n > 1$.

C. Dependence on lattice constant

The results of the previous section show that the dopant merely transfers its electrons to the t_{1u} band, which is thus affected, only because the dopant modifies the lattice constant and the orientational order. Since there is presently no experimental evidence to the contrary, we shall assume that the size of the molecule (its diameter D) is independent of the doping.

The effects of orientation at fixed lattice constant was studied in detail in Sec. III on the basis of TB calculations. The dependence on the lattice constant is much simpler to describe qualitatively, but not quantitatively.

In LDA theory, what matters is the probability for a t_{1u} electron to tunnel from one molecule to the other through the self-consistently determined intermolecular potential barrier. Quantitative calculation of this requires care and computing power, as explained before. On the other hand, the results obtained from one orientational order can be used for another because within the relevant range of lattice constants (14.0 < a < 14.5 Å), the changes of the intermolecular atom-atom distances Δd are much smaller than the intramolecular bond length b, and the latter is again considerably smaller than the intermolecular distances d; specifically, from Eq.(6),

$$\Delta d < b/4 < d/8 . \quad (46)$$

We therefore repeated the LDA calculation for fcc unidirectional RbC_{60}, but with a=14.40 and 14.60 Å (and equal bond lengths). The resulting density of states for the conduction band is shown in Fig. 13 for 14.10 and 14.40 Å. The band shape is virtually unchanged, only the width is decreased by the factor 0.763. For a=14.6 Å

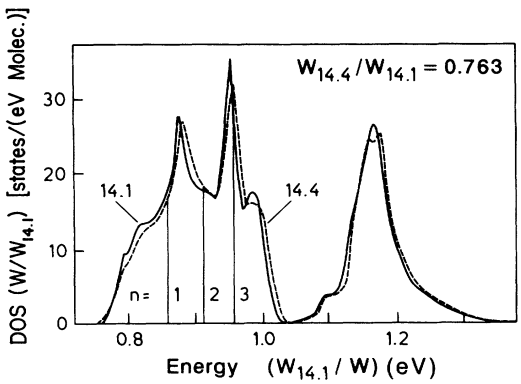

FIG. 13. LDA-LMTO density of states for unidirectional RbC_{60} for two different lattice constants, a=14.1 Å (solid) and a=14.4 Å (dashed). The density of states and energy axes have been scaled with the ratio between the bandwidth (measured at the X point) and the one for 14.1 Å. The energy axis has been shifted so that the Fermi level for two electrons coincides with the one for 14.1 Å. The Brillouin-zone integration was performed with only 18 irreducible k points and equal bond lengths were used. These are the reasons for the deviations from Fig. 8 for a=14.1 Å.

the shape is changed slightly and the width is reduced by a further factor of 0.80. In order to interpolate these results to other lattice constants and to extrapolate them to other orientational orders we return to TB theory.

The change of lattice constant is accounted for in TB theory by changing the hopping integrals V_{12} given by Eq. (12) via change of the interatomic distances d_{12} and directions $\hat{\mathbf{d}}_{12}$. The geometrical considerations necessary to do this were presented in Sec. II. For the relevant range of lattice constants the directional changes in Eq. (12) are negligible, so that the lattice constant enters solely via the distances, that is, via $V[d(a)]$ as given by (13). So far, the parametrization (13) with the parameters (14) was used to describe the hopping at variable distance for one, fixed lattice constant (a=14.1 Å). The lattice-constant dependence calculated in the LDA for the unidirectional structure is, however, also roughly compatible with the form (13), which approximately conserves all ratios between hopping integrals for the lattice constant varying in the relevant range [see (46)] and therefore yields shape-invariant bands. Moreover, the value L=0.505 Å (14) used for the decay constant roughly reproduces the lattice-constant dependence given by the LDA, as we shall now see.

We thus assume that all the conduction-band structures considered for a=14.1 Å scale uniformly in energy when a changes. The bandwidths, the inverse state densities, and all MO-hopping integrals (22) tabulated for the standard lattice constant in Tables II, III, and IV thus scale like

$$V_{\bowtie}(a) = [d_{\bowtie}(a)/d_{\bowtie}]\, V_{\bowtie} \exp[-\{d_{\bowtie}(a) - d_{\bowtie}\}/L], \quad (47)$$

where $d_{\bowtie}(a)$ is the nearest-neighbor distance for contact $\bowtie$, and an omitted argument a indicates that a=14.10 Å. Hence, for the unidirectional and bidirectional structures we may use

$$d_{\parallel}(a) \approx d_{\perp}(a) \approx (a/\sqrt{2}) - 6.95 \text{ Å}, \quad (48)$$

as obtained from Eqs. (7) and (5). For the quadridirectional structure we use

$$d_{\phi}(a)^2 \approx [(a/\sqrt{2}) - 6.85 \text{ Å}]^2 + (0.48 \text{ Å})^2, \quad (49)$$

as obtained from Eq.(10). Adjustment of the L value to fit the LDA results at 14.1 and 14.4 Å yields L=0.63 Å, and adjustment to the results at 14.4 and 14.6 Å yields L=0.54 Å. The LDA decay is thus more gradual than $d\exp(-d/L)$; but it is steeper than a power law d^P because fittings to the LDA results yield $P = -4.1$ and -5.4, in order of increasing lattice constant. We shall take the average value

$$L = 0.58 \text{ Å}. \quad (50)$$

The interpretation of this L value, which is a bit larger than one Bohr radius, is that the orbital energy is a bit more than 13.6 eV below the top of the potential barrier between the molecules. This is consistent with the shape of the LDA potential.

V. COULOMB AND EXCHANGE INTERACTIONS

The simplest estimate of the Coulomb interaction between two electrons in the LUMO is $U = e^2/R \approx 4$ eV. This estimate will be strongly renormalized by "breathing" of the LUMO and by polarization of the surrounding molecules. However, it is unclear whether or not this can reduce U to below the subbandwidth of about 0.5 eV. If not, many-electron effects may modify the intermolecular hopping. Our analytical single-MO model then provides a convenient definition of the kinetic energy in a model Hamiltonian.

One may also ask, how close the doped compounds are to a spin-wave instability? We have evaluated the effective Stoner exchange parameter I for an appropriately renormalized carbon atom in the local spin-density approximation. The result is I = 2.3 eV/(spin C atom), and this means that a ferromagnetic instability does not occur before the density of states at the Fermi level $N(E_F)$ exceeds $2\times60/2.3 = 52$ st./(mol eV). This corresponds roughly to the intermolecular distance d exceeding 3.7 Å.

VI. SUPERCONDUCTIVITY

Fleming *et al.*[24] measured T_c and the lattice constant for a number of n=3 compounds: Rb_2CsC_{60} and several $K_{3-x}Rb_xC_{60}$ compounds. The three data points (a/Å, T_c/K) = (14.253, 19.28), (14.299, 21.80), and (14.436, 29.40) for K_3, K_2Rb, and Rb_3 show particularly little scatter. This is consistent with our expectation that these three compounds are isostructural to a higher degree of accuracy than the other compounds studied, because K^+ is smaller than Rb^+ and the two tetrahedral holes are smaller than the octahedral hole.

It is now tempting to relate these results by the McMillan formula:

$$kT_c = (\hbar\omega/1.2)\exp[-1.04(1+\lambda)/(\lambda-\mu^*-0.62\lambda\mu^*)]. \quad (51)$$

We assume that the relevant phonon modes are intramolecular so that the averaged phonon frequency ω is independent of the intermolecular separation d. Then, by differentiation with respect to d, assuming for simplicity that also the Coulomb-interaction parameter μ^* is independent of the separation, we obtain

$$d\ln T_c/d\lambda = 1.04(1+0.38\mu^*)/(\lambda-\mu^*-0.62\lambda\mu^*)^2. \quad (52)$$

From the three data points we can deduce the two slopes: $d\ln T_c/d\ln d = 11.9$ and 9.9, which relate to the two (geometrical) averages, d= 3.146 and 3.211 Å, of the distances found from (48). Each of these slopes we insert in the numerator on the left-hand side of (52) together with the following values for the denominator: $d\lambda/d\ln d = \lambda d\ln\lambda/d\ln d = \lambda(-1+d/0.58\ \text{Å}) = 4.42\lambda$ and 4.54λ. The latter values are obtained by assuming that $\lambda = N(E_F)V_{e\text{-ph}}$ with a d-independent electron-phonon interaction $V_{e\text{-ph}}$ and by taking the d dependence of the density of states at the Fermi level from the LDA calculations parametrized by Eq.(47).

The differentiated McMillan equation (52) is thus reduced to a relation between λ and μ^* which we solve as a function of μ^*. The resulting values of λ for the two distances, and the average phonon temperatures obtained by substitution into (51) are given in Table V. We see that for all values of μ^*,

$$\omega\hbar/k \approx 600\ \text{K}.$$

This value for the average phonon frequency seems consistent with the assumption that the relevant modes be intramolecular. In fact, it is near the low-lying $H_g(2,z)$ radial mode.[25]

However, for the results to be consistent with our assumptions about a d-independent average phonon frequency and electron-phonon interaction, we should have $|d\ln V_{e\text{-ph}}/d\ln N(E_F)| \ll 1$ and $|d\ln\omega/d\ln T_c| \ll 1$. This is not really satisfied for any value of μ^*, although $d\ln V_{e\text{-ph}}/d\ln N(E_F)$ seems to reach a minimum of 0.2 around $\mu^* \approx 0.5$. We must therefore conclude that at least one of the interactions, the electron-electron or the electron-phonon, must be in part intermolecular. For either interaction there are good reasons why this should be true.

We would finally like to point out that the considerations above do not depend on the absolute value of $N(E_F)$, but only on its lattice-constant dependence. Our calculated absolute values obtained from Fig. 8 and Eq. (47) are $N(E_F)$ = 17.2, 18.0, and 20.5 st./(mol eV) for K_3C_{60}, K_2RbC_{60}, and Rb_3C_{60} in the unidirectional structure, and about 10% larger in the bidirectional structure. This value for unidirectional K_3C_{60} is somewhat larger than the value 13.2 st./(mol eV) obtained in a recent LCAO calculation.[23]

TABLE V. Electron-phonon coupling constant λ and average phonon frequency ω as functions of the Coulomb-interaction parameter μ^*, obtained as described in the text using experimental T_c data and the dependence of $N(E_F)$ on lattice constant given by the LDA (L=0.58 Å). Columns (a): T_c = 20.50 K, d = 3.146 Å. Columns (b): T_c = 25.32 K, d = 3.211 Å.

μ^*	λ		$\frac{d\ln V_{e\text{-ph}}}{d\ln N(E_F)}$	$\omega\hbar/k$ (K)		$\frac{d\ln\omega}{d\ln T_c}$
	(a)	(b)		(a)	(b)	
0.15	0.79	0.91	0.54	650	572	−0.61
0.25	1.11	1.25	0.37	603	552	−0.42
0.35	1.47	1.65	0.26	604	565	−0.32
0.45	1.92	2.14	0.21	637	604	−0.25

VII. SUMMARY

In this paper we have considered pure and alkali-metal-doped fcc C_{60} for three different cases of orientational order, the simple unidirectional structure, an equal-composition bidirectional ordered structure which, in its random form, is the structure of alkali-metal-doped C_{60} at room temperature, and the low-temperature quadridirectional structure of pure C_{60}. After a detailed discussion of the geometries in the regions of contact between the C_{60} molecules, we have calculated and discussed the conduction-band structures, first in the TB approximation and then in the LDA.

The coefficients of the radially oriented carbon orbitals for the t_{1u} molecular orbitals could be found analytically and, on the basis of these, we derived analytical expressions for the conduction-band Hamiltonians for the three structures; their dimensions are, respectively, 3×3, 6×6, and 12×12. Although these t_{1u} Hamiltonians neglect the hybridization with subbands derived from other molecular orbitals, they gave quite accurate bands *and* they could be used to fit the conduction-band structures calculated with less approximative methods, the TB method in the 60 radial-orbitals approximation, and the *ab initio* LDA-LMTO method. The hopping parameters of this t_{1u} model were listed in Tables II, III, and IV. The details of the band dispersions were then discussed and related to the contact geometries. The densities of states were shown in Figs. 6–8 and the bands in Figs. 4, 5, 9, and 10.

We then studied the effects of alkali-metal doping and the associated change of the lattice constant by performing *ab initio* LDA calculations for the simplest structure. Specifically, we treated unidirectional fcc C_{60} and RbC_{60} for three different lattice constants (a=14.1, 14.4, and 14.6 Å) using the LMTO-ASA method with carefully chosen interstitial spheres. Comparison with photoemission and inverse photoemission data for C_{60} gave reasonable agreement for the subband positions and widths. For AC_{60}, we found that the alkali-metal atom is fully ionized and that the doped electrons occupy the t_{1u} band

in a rigid-band-like fashion. Crude tight-binding estimates using our analytical t_{1u} orbital explained why this is so. As a function of the lattice constant and for a given structure, the conduction band was found to scale uniformly in energy with the energy scale behaving like $W \propto d(a)\exp[-d(a)/0.58\ \text{Å}]$, where d is the distance between nearest atoms on different molecules and is given by (48) or (49). For a=14.1 Å the conduction-band widths were found to be 0.52 eV (uni), 0.64 (bi), and 0.44 eV (quadri). The density of states at the Fermi level for K_3C_{60}, K_2RbC_{60}, and Rb_3C_{60} was 17.2, 18.0, and 20.5 st./(mol eV) in the unidirectional structure and about 10% larger in the bidirectional structure.

Evaluation of the LDA Stoner exchange parameter yielded $I \approx 2.3$ eV/(spin·atom), meaning, for instance, that in order to reach a spin-density-wave instability, the intermolecular separation should be increased to about 3.7 Å. The Coulomb self-energy for a molecular orbital is presumably several times the LDA bandwidths, and future studies must take this into account. Finally, we used the LDA value 0.58 Å for the decay of the intermolecular hopping together with experimental data for T_c versus lattice constant for $K_{3-x}Rb_xC_{60}$ compounds in the McMillan formula. It was found that our assumptions that the Coulomb interaction μ^*, the electron-phonon interaction $V_{e\text{-ph}}$, and the average phonon frequency ω be independent of the lattice constant cannot all be true.

ACKNOWLEDGMENTS

Inspiring discussions with H. G. von Schnering, L. Schroeder, and I.I. Mazin are gratefully acknowledged. One of us (A.I.L.) was supported by the A. von Humbold foundation.

*Permanent address: Department of Physics and Astronomy, University of Missouri, Columbia, MO 65211.
†Permanent address: Institute of Physics of Metals, Yekaterinburg, Russia.
‡Permanent address: Institute of Chemistry, Yekaterinburg, Russia.

[1] H. W. Kroto *et al.*, Nature (London) **318**, 162 (1985).
[2] W. Krätschmer, L. D. Lam, K. Fostiropoulos, and D. R. Huffman, Nature (London) **347**, 354 (1990).
[3] A. F. Hebard *et al.*, Nature (London) **350**, 600 (1991); K. Holczer *et al.*, Science **252**, 1154 (1991); M. J. Rosseinsky *et al.*, Phys. Rev. Lett. **66**, 2830 (1991).
[4] P. A. Heiney *et al.*, Phys. Rev. Lett. **66**, 2911 (1991).
[5] R. Sachidanandam and A. B. Harris, Phys. Rev. Lett. **67**, 1467 (1991).
[6] W. I. F. David *et al.*, Nature (London) **353**, 147 (1991).
[7] P. W. Stephens *et al.*, Nature (London) **351**, 632 (1991).
[8] P. J. Benning *et al.*, Science **252**, 1417 (1991).
[9] K. Tanigaki *et al.*, Nature **352**, 222 (1991).
[10] R. M. Fleming (private communication).
[11] T. Takahashi *et al.*, Physica C **185-189**, 417 (1991).
[12] S. Satpathy, Chem. Phys. Lett. **130**, 545 (1986).
[13] R. C. Haddon, L. E. Brus, and K. Raghabachari, Chem. Phys. Lett. **125**, 459 (1986).
[14] S. Saito and A. Oshiyama, Phys. Rev. Lett. **66**, 2637 (1991).
[15] O. Gunnarsson, S. Satpathy, O. Jepsen, and O. K. Andersen, Phys. Rev. Lett. **67**, 3002 (1991).
[16] W. A. Harrison, *Electronic Structure and the Properties of Solids* (Dover, New York, 1989).
[17] O. K. Andersen, Z. Pawlowska, and O. Jepsen, Phys. Rev. B **34**, 5253 (1986), W. R. L. Lambrecht and O. K. Andersen, *ibid.* **34**, 2439 (1986); A. T. Paxton, M. Schilfgaarde, O. K. Andersen, and O. Jepsen (unpublished).
[18] J. H. Weaver *et al.*, Phys. Rev. Lett. **66**, 1741 (1991); P. J. Benning *et al.*, Phys. Rev. B **44**, 1962 (1991).
[19] M. B. Jost *et al.*, Phys. Rev. B **44**, 1966 (1991).
[20] P. Baltzer *et al.* (unpublished).
[21] R. W. Lofet *et al.* (unpublished).
[22] J. L. Martins, N. Troullier, and M. Schabel (unpublished).
[23] S. C. Erwin and W. E. Pickett, Science **254**, 842 (1991).
[24] R. M. Fleming *et al.*, Nature **352**, 787 (1991).
[25] G. B. Adams *et al.*, Phys. Rev. B **44**, 4052 (1991).

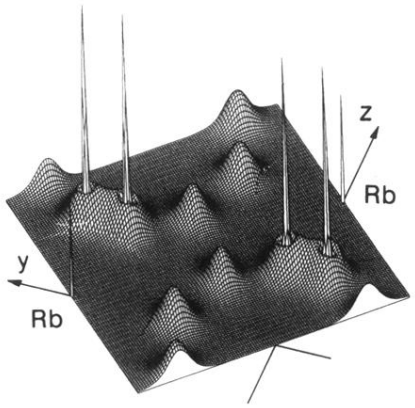

FIG. 12. Valence charge-density in the yz plane (see Fig. 2) for RbC_{60} in the fcc unidirectional structure. The plane passes through the Rb octahedral sites and, for each of two neighboring molecules, it contains a top hexagon edge and passes between two contact atoms plus the midpoint of another top hexagon edge. The Rb $5s$ electron is seen to be transferred to the C_{60} molecule.